Department of Micro- and Nanosciences

Atomic layer deposited titanium dioxide in optical waveguiding applications

Tapani Alasaarela

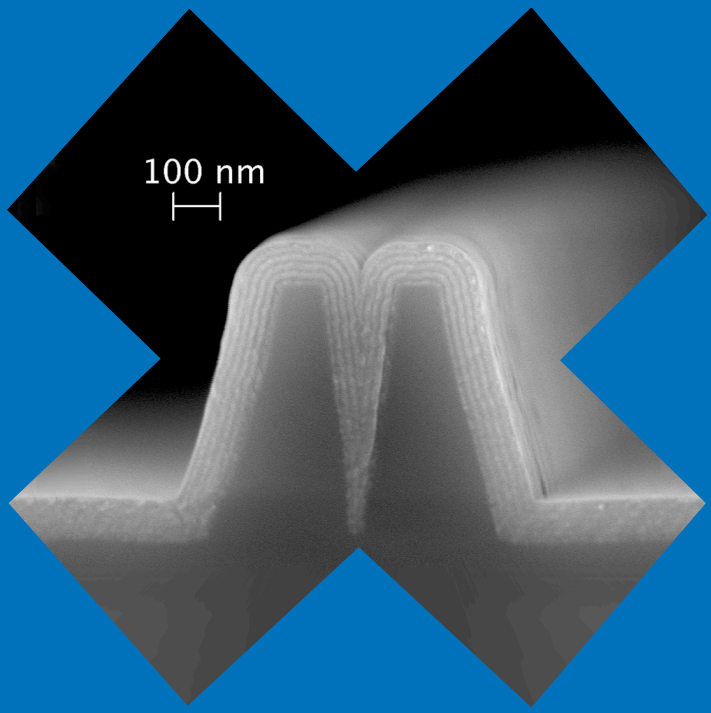

Aalto University

DOCTORAL DISSERTATIONS

Aalto University publication series
DOCTORAL DISSERTATIONS 57/2011

Atomic layer deposited titanium dioxide in optical waveguiding applications

Tapani Alasaarela

Doctoral dissertation for the degree of Doctor of Science in Technology to be presented with due permission of the Aalto University School of Electrical Engineering for public examination and debate in the lecture hall AS1 of the TUAS building (Otaniementie 17, Espoo, Finland) at Aalto University School of Electrical Engineering on the 29th of June 2011 at 12 o'clock.

Aalto University
School of Electrical Engineering
Department of Micro- and Nanosciences
Photonics Group

Supervisor
Prof. Seppo Honkanen

Preliminary examiners
Dr. Pekka Äyräs, Nokia Research Center, Finland
Prof. Robert Norwood, University of Arizona, USA

Opponent
Dr. Laurent Vivien, L'Université Paris-Sud, France

Aalto University publication series
DOCTORAL DISSERTATIONS 57/2011

ISBN 978-952-60-4180-3 (pdf)
ISBN 978-952-60-4179-7 (printed)
ISSN-L 1799-4934
ISSN 1799-4942 (pdf)
ISSN 1799-4934 (printed)

Aalto Print
Helsinki 2011

Finland

The dissertation can be read at http://lib.tkk.fi/Diss/

Author
Tapani Alasaarela

Name of the doctoral dissertation
Atomic layer deposited titanium dioxide in optical waveguiding applications

Publisher School of Electrical Engineering

Unit Department of Micro- and Nanosciences

Series Aalto University publication series DOCTORAL DISSERTATIONS 57/2011

Field of research Photonics

Manuscript submitted 6 April 2011 **Manuscript revised** 13 June 2011

Date of the defence 29 June 2010 **Language** English

☐ **Monograph** ☒ **Article dissertation (summary + original articles)**

Abstract

This thesis introduces the use of atomic layer deposited (ALD) amorphous titanium dioxide (TiO2) in various waveguiding applications. The ALD of amorphous TiO2 is done by sequential pulsing of titanium tetrachloride (TiCl4) and water vapors into a nitrogen carrier gas flow at relatively low deposition temperatures of below 120°C and in a medium vacuum. The optical properties of the amorphous TiO2 slab waveguides are studied in the visible and near-infrared wavelengths, and a propagation loss of < 1 dB/cm at 1.55 micrometer wavelength is measured. The conformal growth mode of ALD is used to narrow down silicon slot and to smoothen waveguide edges with an amorphous TiO2 layer, which enables fabrication of silicon slot waveguides with thin air slots and relatively low losses of down to 7 dB/cm.

ALD-TiO2 is also used to successfully fabricate novel absorbing polarization selective resonant gratings, and semi-wide bandwidth resonant waveguide reflectors. A novel way of fabricating a resonant waveguide grating by applying an ALD-TiO2 layer on a holographically written surface relief grating on an azobenzene polymer complex is introduced. Amorphous ALD-TiO2 shows an excellent performance in all the studied applications, and will very probably see use in various photonic devices in the future. The low growth temperature allows the fabrication of ALD-TiO2 waveguides on top of processed microchips, so ALD-TiO2 might also turn out to be a suitable material in building the optically interconnected microchips of the future.

Keywords atomic layer deposition, waveguide, silicon photonics, grating, titanium dioxide

ISBN (printed) 978-952-60-4179-7 **ISBN (pdf)** 978-952-60-4180-3

ISSN-L 1799-4934 **ISSN (printed)** 1799-4934 **ISSN (pdf)** 1799-4942

Location of publisher Espoo **Location of printing** Helsinki **Year** 2011

Pages 139 **The dissertation can be read at** http://lib.tkk.fi/Diss/

Aalto-yliopisto

Tiivistelmä

Aalto-yliopisto, PL 11000, 00076 Aalto www.aalto.fi

Tekijä
Tapani Alasaarela

Väitöskirjan nimi
Atomikerroskasvatettu titaanidioksidi optisissa aaltojohdesovelluksissa

Julkaisija Sähkötekniikan korkeakoulu

Yksikkö Mikro- ja nanotekniikan laitos

Sarja Aalto University publication series DOCTORAL DISSERTATIONS 57/2011

Tutkimusala Fotoniikka

Käsikirjoituksen pvm 06.04.2011 **Korjatun käsikirjoituksen pvm** 13.06.2011

Väitöspäivä 29.06.2010 **Kieli** Englanti

☐ **Monografia** ☒ **Yhdistelmäväitöskirja (yhteenveto-osa + erillisartikkelit)**

Tiivistelmä

Väitöskirjassa on tutkittu titaanidioksidin (TiO2) kasvattamista atomikerroskasvatuksella (ALD) amorfisiksi ohutkalvoiksi käytettäviksi erilaisissa aaltojohdesovelluksissa. Käytetty ALD-prosessi perustuu titaanitetrakloridin (TiCl4) ja veden vuoronperäiseen pulssitukseen matalissa alle 120 °C lämpötiloissa. Kemikaalit pulssitetaan tyhjiössä reaktiokammion läpi virtaavaan typpeen. Amorfisten TiO2-kalvojen optisia ominaisuuksia tasoaaltojohteena tutkittiin ja suhteellisen pienet alle 1 dB/cm etenemishäviöt mitattiin 1.55 mikrometrin aallonpituudella. ALD-menetelmän pintoja myötäilevää kasvua käytettiin piislot-valokanavien kaventamiseen ja reunojen pehmentämiseen, ja täten saatiin valmistettua suhteellisen pienihäviöisiä ilmatäytteisiä slotvalokanavia. Parhaassa ilmatäytteisessä slotvalokanavassa etenemishäviö oli 7 dB/cm.

Amorfisia TiO2-kalvoja käytettiin myös uudenlaisen absorboivan polarisaatioselektiivisen resonanssiaaltojohdehilan ja laajakaistaisen resonanssiaaltojohdehilaheijastimen valmistamiseen. Työssä esitellään myös uusi tapa valmistaa resonanssiaaltojohdehiloja kasvattamalla ALD-TiO2-kalvo holografisesti kuvioidun atsobentseenipintahilan päälle. Amorfinen ALD-TiO2 toimi erinomaisesti kaikissa tutkituissa sovelluksissa ja sitä tullaan erittäin todennäköisesti soveltamaan useissa erilaisissa fotoniikkakomponenteissa tulevaisuudessa. Matala kasvatuslämpötila mahdollistaa ALD-TiO2 valokanavien valmistamisen prosessoitujen mikropiirien päälle, joten ALD-TiO2 voisi olla soveltuva materiaali käytettäväksi tulevaisuuden mikropiirien sisäisessä optisessa tiedonsiirrossa.

Avainsanat atomikerroskasvatus, aaltojohde, piifotoniikka, hila, titaanidioksidi

ISBN (painettu) 978-952-60-4179-7 **ISBN (pdf)** 978-952-60-4180-3

ISSN-L 1799-4934 **ISSN (painettu)** 1799-4934 **ISSN (pdf)** 1799-4942

Julkaisupaikka Espoo **Painopaikka** Helsinki **Vuosi** 2011

Sivumäärä 139 **Luettavissa verkossa osoitteessa** http://lib.tkk.fi/Diss/

Preface

When I was a small child, I used to play with different substances we had in our kitchen and tried to develop new kind of substances, and wanted to become a chemist one day. A bit later on I become more interested in computers and decided that one day I would like to understand and design microprocessors. Both of these childhood dreams have become partly reality, as I happened to start working on a chemical process, and my thesis work has also a touch of silicon processing, and maybe helps one step towards realizing the optical interconnects on a silicon microchip. The journey this far has been fascinating, and there are a whole lot of people I am thankful for helping me surpass myself and reach my ambitious goals.

This study is a result of slightly less than three years of research conducted at Department of Micro- and Nanosciences in Aalto University School of Electrical Engineering (formerly Helsinki University of Technology), where I have had the honor to work under Professor Seppo Honkanen's supervision. I am very grateful to Seppo for the encouragement, helpful discussions, and for all the great and not-so-great ideas we had and that he allowed me to pursue on my own will.

During the years I have also had an opportunity to do some side work at Beneq Oy, which has given me some industrial perspective and access to huge amount of knowledge on atomic layer deposition. Especially, I want to thank Jarmo Maula for introducing me to the fascinating world of atomic layer deposition (ALD), while I was doing my Master's thesis, and for all the fun and educating discussions we have had over years. Also, I want to acknowledge Olli Jylhä, Matti Putkonen, Milja Mäkelä, Ville Malinen, Nora Isomäki, Sami Sneck, Pekka Soininen and other colleagues at Beneq who have helped me to get forward and given great insights.

I want to express my warm thanks to Ari Tervonen and Antti Säynätjoki for sharing their knowledge in optics and co-authoring many of my pub-

lications. I am also grateful for my colleagues Markus Bosund, Lasse Karvonen, Henri Jussila, Päivi Mattila, Marco Mattila, Pasi Kostamo, Nikolai Chekurov, Amit Khanna, Ya Chen, Joan Montiel and Lauri Riuttanen for helping in servicing the equipment, setting up experiments, teaching me how to use the equipment new to me, and for all the nice discussions we have shared during these years. I acknowledge also Arri Priimägi for introducing me to the world of azobenzene polymers. I would also like to thank all my co-authors at VTT Oulu, University of Eastern Finland, Tsinghua University, and Karlsruhe Institute of Technology.

I would like to thank my sources of funding, namely the Graduate School of Modern Optics and Photonics, Walter Ahlström Foundation, Emil Aaltonen Foundation, and KAUTE Foundation for the financial support which has helped me through the studies. I also acknowledge Beneq Oy for covering a part of the printing costs of this thesis.

Finally, I would like to express my gratitude to my parents and siblings for their love and support throughout my life. And my dear Anne, thank you for your love and caring during the last years.

Helsinki, June 14, 2011,

Tapani Alasaarela

Contents

List of Publications

This thesis consists of an overview and of the following publications which are referred to in the text by their Roman numerals.

I T. Alasaarela, A. Säynätjoki, T. Hakkarainen, and S. Honkanen. Feature size reduction of silicon slot waveguides by partial filling using atomic layer deposition. *Optical Engineering*, vol. 48, no. 8, pp. 080501-1–3, August 2009.

II A. Säynätjoki, T. Alasaarela, A. Khanna, L. Karvonen, P. Stenberg, M. Kuittinen, A. Tervonen, and S. Honkanen. Angled sidewalls in silicon slot waveguides: conformal filling and mode properties. *Optics Express*, vol. 17, no. 23, pp. 21066–21076, November 2009.

III T. Alasaarela, D. Korn, L. Alloatti, A. Säynätjoki, A. Tervonen, R. Palmer, J. Leuthold, W. Freude, and S. Honkanen. Reduced propagation loss in silicon strip and slot waveguides coated by atomic layer deposition. *Optics Express*, vol. 19, no. 12, pp. 11529–11538, June 2011.

IV T. Alasaarela, T. Saastamoinen, J. Hiltunen, A. Säynätjoki, A. Tervonen, P. Stenberg, M. Kuittinen, and S. Honkanen. Atomic layer deposited titanium dioxide and its application in resonant waveguide grating. *Applied Optics*, vol. 49, no. 22, pp. 4321–4325, August 2010.

V A. Lehmuskero, I. Vartiainen, T. Saastamoinen, T. Alasaarela, and M. Kuittinen. Absorbing polarization selective resonant gratings. *Optics Express*, vol. 18, no. 26, pp. 27270–27279, December 2010.

VI T. Saastamoinen, T. Alasaarela, A. Lehmuskero, I. Vartiainen, N. Heikkilä, and M. Kuittinen. Resonance waveguide reflectors with semi-wide bandwidth at the visible wavelengths. *Optics Express*, vol. 19, no. 3, pp. 2126–2132, January 2011.

Some of the results in this thesis have also been presented in the following publication:

[1] T. Alasaarela, D. Zheng, L. Huang, A. Priimagi, B. Bai, A. Tervonen, S. Honkanen, M. Kuittinen, and J. Turunen, Single-layer one-dimensional nonpolarizing guided-mode resonance filters under normal incidence. *Optics Letters*, In press.

and in following conferences and conference proceedings:

[2] A. Säynätjoki, L. Karvonen, A. Khanna, T. Alasaarela, A. Tervonen, S. Honkanen, Silicon slot waveguides for nonlinear optics, *Proc. SPIE*, vol. 7212, 72120T, 2009.

[3] T. Alasaarela, A. Säynätjoki, P. Stenberg, M. Kuittinen, S.Honkanen, Filling of Slot Waveguides with Atomic Layer Deposition (talk), *CLEO Europe -EQEC 2009*, Munich, Germany, June 14-19, Paper CK10.6, 2009.

[4] T. Alasaarela, A. Säynätjoki, P. Stenberg, M. Kuittinen, S. Honkanen, Filling of Slot Waveguides with Versatile Material Systems Using Atomic Layer Deposition (poster), *Integrated Photonics and Nanophotonics Research and Applications (IPNRA)*, Honolulu, Hawaii, USA, July 12-17, Paper JTuB4, 2009.

[5] A. Säynätjoki, T. Alasaarela, A. Khanna, L. Karvonen, A. Tervonen, S. Honkanen, Advantages of Angled Sidewalls in Slot Waveguides (talk), *Integrated Photonics and Nanophotonics Research and Applications (IPNRA)*, July 12-17, Honolulu, Hawaii, USA, Paper ITuE2, 2009.

[6] T. Alasaarela, J. Hiltunen, A. Khanna, A. Säynätjoki, A. Tervonen, S. Honkanen, Optical properties of atomic layer deposited materials and their application in silicon waveguides, Proc. SPIE vol. 7598, 75980D, 2010.

[7] A. Säynätjoki, T. Alasaarela, A. Khanna, A. Tervonen, S. Honkanen, Mode properties of ALD filled silicon slot waveguides, *Proc. SPIE*, vol. 7606, 76061G, 2010.

[8] T. Alasaarela, A. Priimägi, B. Bai, A. Tervonen, S. Honkanen, Titanium dioxide coated photoinduced surface relief grating as a resonant waveguide grating (talk), *CLEO Europe -EQEC 2011*, Munich, Germany, May 22-26, Paper CE8.1, 2011.

Author's Contribution

Publication I: "Feature size reduction of silicon slot waveguides by partial filling using atomic layer deposition"

The author did most of the theoretical work, most of the experiments, and prepared the manuscript. The patterning of silicon wafers was done in University of Joensuu.

Publication II: "Angled sidewalls in silicon slot waveguides: conformal filling and mode properties"

The author contributed in the theoretical work, did the experimental work except the patterning of silicon wafers, and contributed in writing of the manuscript.

Publication III: "Reduced propagation loss in silicon strip and slot waveguides coated by atomic layer deposition"

The author did most of the theoretical work, the ALD processing and SEM characterizations, and prepared the manuscript.

Publication IV: "Atomic layer deposited titanium dioxide and its application in resonant waveguide grating"

The author did the theoretical work apart from the resonant waveguide grating part, most of the ALD processing and SEM characterizations, and prepared most of the manuscript.

Publication V: "Absorbing polarization selective resonant gratings"

The author contributed in the development of experimental processes, did the ALD processing and contributed in writing of the manuscript.

Publication VI: "Resonance waveguide reflectors with semi-wide bandwidth at the visible wavelengths"

The author did the ALD processing part of the experiments and contributed in writing of the manuscript.

1. Introduction

The understanding of the physics of light has evolved a lot in the course of history. Through the work of Max Planck, Albert Einstein, Louis de Broglie, Arthur Compton, Niels Bohr, and many others, we have learned that all particles have a wave nature and all waves have a particle nature. We have understood that light and other electromagnetic waves take the form of photons, which are quantized, self-propagating oscillatory electromagnetic field perturbations. Both the terms optics and photonics are used when referring to the physics of light, usually emphasizing classical applications (lenses, telescopes, cameras, etc.) with the term optics and modern applications (semiconductors, optical fibers, waveguides, gratings, etc.) with photonics.

Silicon has become the material of microelectronics, and the fabrication techniques have evolved greatly over recent decades. Silicon has many useful features which have enabled its wide adoption: suitable electronic properties, stable and electrically insulating natural oxide, and nearly unlimited supply. Because of the wide adoption and mature fabrication processes of the silicon platform, it is highly promising to exploit the same technology also for photonics [9]. Silicon is transparent at wavelengths above $\sim$1.2 μm, which is convenient as the optical fibers used in telecommunications typically operate at wavelengths near 1.55 μm. Silicon photonics could also provide a chip-scale platform for monolithic integration of optics and microelectronics in the same chip [10, 11].

The silicon photonic devices are based on similar silicon-on-insulator (SOI) substrates that were originally developed for microelectronics. A typical SOI wafer for photonic applications has a 220 nm thick single crystalline silicon device layer on top of a 2 μm thick buried oxide (BOX) on a 500 μm thick silicon base wafer. Laterally confining waveguide structures can be easily etched on the device layer as the BOX can be used as

a natural etch stopper. In this thesis, I have studied the silicon strip and slot waveguides and the modification of their properties by atomic layer deposition (ALD).

As well as silicon, also silicon nitride (Si_3N_4) has been used to fabricate waveguides working at wavelengths ranging from visible to infrared wavelengths. Si_3N_4 is often grown in high temperatures using various chemical vapor deposition (CVD) methods, but also lower temperature plasma enhanced chemical vapor deposition (PECVD) method.

ALD is a thin film deposition technique, which was invented independently by different researchers in the Soviet Union and in Finland. Tuomo Suntola invented it especially for making thin film electroluminescent (TFEL) displays in 1974. The technology was first named atomic layer epitaxy (ALE) and molecular layering (ML), but the name ALD has been commonly adopted as it describes the technology more accurately. Other names used for the technique include atomic layer chemical vapour deposition (ALCVD), and molecular layer epitaxy (MLE). A longer overview of the history can be found in Puurunen's review [12].

ALD has recently gained a lot of interest in many different applications. In 1990s it was adopted by the semiconductor industry for depositing thin dielectric films and since 2000, it has also been applied to photovoltaics and barrier applications. In this thesis, the focus is on the photonics applications of ALD, and especially its use in different waveguide and grating applications.

Diffraction gratings are periodic structures that consist of nano- or micrometer-sized features. In a resonance waveguide grating (RWG), light is coupled between the guided and diffracted modes forming sharp spectral resonance peaks, where light is either completely transmitted or reflected. A waveguide grating coupler is an important element of the silicon photonic platform, as it enables coupling of light between an optical fiber and the photonic chip with a simple coupling scheme. As well as on silicon, gratings are routinely fabricated on different kinds of glasses, polymers, and other substrates.

In this thesis the use of ALD-TiO_2 in waveguiding applications is studied. In the publications included, we have proposed narrowing of slot waveguides with ALD-TiO_2 [Publication I], estimated the effects of completely filling angled silicon slot waveguide structures [Publication II], measured the waveguiding properties of amorphous TiO_2 [Publication IV], and demonstrated reduction of losses in strip and slot waveguides

by the same TiO_2 material [Publication III]. We have also demonstrated ALD-TiO_2 in various grating structures [Publications IV,V,VI].

In Chapter 2, a literature study on optical properties of ALD materials and different optical applications of ALD is given. Also, some industrial aspects of ALD are discussed in Section 2.4. Chapter 3 gives an overview of the theoretical basis used in the thesis starting from Maxwell's equations and then explaining various different methods for analyzing thin films, waveguides, and gratings theoretically.

The experimental methods are explained in Chapter 4. The patterning of nanostructures, ALD processing of TiO_2 and various characterization methods are described. The results from the publications, and additionally a completely TiO_2-filled slot waveguide and a novel azobenzene resonant waveguide grating structure are presented in Chapter 5, and finally the summary and outlook are given in Chapter 6.

2. Atomic layer deposition in optical applications

2.1 Optical properties of ALD materials

The history of optical ALD films goes back all the way to its invention in Finland. Thin film electroluminescent (TFEL) displays needed better phosphors and dielectric film stacks, and ALD came in to help in making pin-hole free and high quality films. Since then, its usage in different optical applications has widened to optical filters, and many different kinds of optical nanostructures.

Although ALD was invented for making TFEL displays, the late material research has focused much more on the electrical rather than optical properties of ALD materials. Thus, it is often quite difficult to find optical parameters of ALD materials and good processes for different optical or photonics applications.

The optical properties of crystalline materials are strongly dependent on the crystal structure of the material. ALD grown TiO_2 can be amorphous or crystalline depending on the growth temperature and their optical properties are quite different. The refractive index can vary from about 2.2 of amorphous TiO_2 to 2.65 of preferentially oriented anatase (at a wavelength of 633 nm) [13]. Crystalline materials tend to have high scattering losses, if the crystal size is more than a few nanometers. This can be prevented by applying thin intermediate layers. Adding intermediate Al_2O_3 layers to crystalline TiO_2 increases the specular transmittance and the material appears optically amorphous [14]. This thesis focuses on low temperature titanium tetrachloride ($TiCl_4$) + water process that gives high quality amorphous TiO_2 films. The process is explained in Section 4.3.

ALD offers an ability to create artificial materials with custom refractive index between the high and low index materials. This ability has been

used in making an optical retarder [15]. However, finding suitable processes for nanolaminates can be difficult as intermediate materials with unwanted properties might be formed at the interfaces. For example, we have found that nanolaminate films done by mixing trimethylaluminium (TMA) + water and $TiCl_4$ + water processes are absorbing. This is due to some other interfacial effects, as the amount of absorption increases quite linearly with the number of interfaces.

In telecommunication applications, the most important wavelengths are in 1.3–1.6 μm range. Unfortunately, not much information about the optical properties of ALD materials at these wavelengths is readily available. In waveguide applications, light is usually propagating centimeters instead of hundreds of nanometers or a few micrometers as in optical coatings, so the quality requirements are more demanding.

A list of ALD processes with refractive indices, precursor chemicals, process temperatures and growth rates is shown in tables 2.1 and 2.2.

Table 2.1. Optical properties of ALD materials and the used precursor chemicals. The processes marked with * are not good ALD processes and have high nonuniformities.

Material	Refractive index	Precursor chemicals	Process Temperature	Growth rate (ÅĚ/cycle)	Ref.	
La_2S_3	2.7-2.8	$La(thd)_3 + H_2S$	300-500	0.1-0.2	[16]	
TiO_2	2.2-2.8	$TiCl_4 + H_2O$	100-600	0.3-1.5	[13, 17, 18] [19],[IV]	
		$Ti(OCH(CH_3)_2)_4 + H_2O$	150-350	0.1-0.6	[20]	
		$Ti(OCH_2CH_3)_4 + H_2O$	250-400	0.3-1.2	[21]	*
		$TiI_4 + H_2O_2$	250-490	0.3-1.2	[22]	
In_2S_3	2.5-2.7	$InCl_3 + H_2S$	300-400	1.4	[23]	
		$In(acac)_3 + H_2S$	140-280	0.2-0.7	[24]	
Cr_2O_3	2.4-2.7	$CrO_2Cl_2 + CH_3OH$	330-465	0.5-1.0	[25]	
$ZnS_{1-x}Se_x$	2.3-2.5	$ZnCl_2 + H_2S +$ Se	400, 500	0.8-1.3	[26, 27]	
NiO	2.4	$Ni(C_5H_5)_2 + O_3$	300	not stated	[28]	
Nb_2O_5	2.2-2.4	$Nb(OC_2H_5)_5 + H_2O$	150-350	0.1-0.3	[29]	*
ZnS	2.3	$ZnCl_2 + H_2S$	500	0.8-1.0	[30, 31]	
		$ZnOAc + H_2S$	320	1.7-1.8	[32]	
ZrO_2	1.8-2.3	$ZrCl_4 + H_2O$	500	0.1-0.5	[33]	
		$Zr[OC(CH_3)_3]_4 + H_2O$	150-300	0.1-1.9	[34]	
		$ZrI_4 + H_2O$-H_2O_2	250-500	0.3-1.3	[35, 36]	
		$[Zr(O^tBu)_2(dmae)_2]_2 + H_2O$	190-340	0.6-1.3	[37]	
$SrS_{1-x}Se_x$	2.1-2.2	$Sr(thd)_2 + H_2S +$ Se	380	not stated	[27]	
Ta_2O_5	1.9-2.2	$TaCl_5 + H_2O$	80-500	0.4-1.6	[38]	*
CaS	2.1	$Ca(thd)_2 + H_2S$	325-400	0.1-0.5	[39]	

Table 2.2. Optical properties of ALD materials and the used precursor chemicals. The processes marked with * are not good ALD processes and have high nonuniformities. (Table 2.1 continued.)

Material	Refractive index	Precursor + chemicals	Process Temperature	Growth rate (ÅĖ/cycle)	Ref.	
BaS	2.1	$Ba(thd)_2 + H_2S$	275-400	0.6-0.9	[40]	
		$(C_5Me_5)_2Ba(THF)_x + H_2S$	180-400	1.2-1.9	[41]	
In_2O_3	2.1	$InCl_3 + H_2O$	400, 500	0.1-0.3	[42]	
		$InCl_3 + H_2O_2$	300, 500	0.2-0.4	[43]	
SrS	2.0-2.1	$Sr(thd)_2 + H_2S$	350-450	0.3-1.2	[44]	
		$(C_5^iPr_3H_2)_2Sr(THF) + H_2S$	120-460	0.6-3.0	[41]	*
		$(C_5Me_5)_2Sr(THF)_x + H_2S$	155-400	0.8-1.6	[41]	
Si_3N_4	2.0-2.1	$SiCl_4 + NH_3$	227-627	1.4-2.5	[45]	*
$SrTa_2O_6$	1.9-2.1	$SrTa_2(OEt)_{10}(dmae)_2 + H_2O$	200-350	0.2-0.3	[46]	
HfO_2	1.8-2.1	$HfCl_4 + H_2O$	300, 500	0.4-0.6	[47, 48]	
		$HfI_4 + H_2O$	300	0.4-0.6	[48]	
		$Hf(OCMe_2CH_2OMe)_4 + H_2O$	275-425	0.1-1.0	[49]	
		$TEMAHf + O_3$	160-370	0.7-1.1	[50]	
ZnO	2.0	$DEZ + H_2O$	177	2.0	[51]	
AlN	2.0	$AlCl_3 + NH_3$	500	1.0	[52]	
Sc_2O_3	2.0	$Sc(thd)_3 + O_3/H_2O$-H_2O_2	275-500	0.1-0.2	[53]	
		$(C_5H_5)_3Sc + H_2O$	175-500	0.7-0.8	[53]	
Gd_2O_3	1.9-2.0	$Gd[OC(CH_3)_2CH(CH_3)_2]_3 + H_2O$	300-400	0.3-0.5	[54]	
$LaGaO_3$	1.9-2.0	$La(thd)_3/Ga(acac)_3 + O_3$	325-425	0.4	[55]	
SnO_2	1.6-2.0	$SnCl_4 + H_2O$	300-600	0.1-0.3	[56]	
		$TDMASn + O_3/H_2O_2/H_2O$	50-325	0.6-1.6	[57]	
Y_2O_3	1.8-1.9	$Y(thd)_3 + O_3$	200-600	0.2-0.8	[58, 59]	
Ga_2O_3	1.8-1.9	$Ga(acac)_3 + O_3/H_2O$	370	0.2-0.3	[60]	
ITO	1.8-1.9	$InCl_3/SnCl_4 + H_2O$	500	0.2	[61]	
		$InCl_3/SnCl_4 + H_2O_2$	300,500	0.3	[43]	
$PrSiO_x$	1.8-1.9	$Pr[N(SiMe_3)_2]_3 + H_2O$	200-400	0.2-1.1	[62]	*
Lu_2O_3	1.8-1.9	$Lu(iPrO)_3 + H_2O$	330	not stated	[63]	
$LaAlO_3$	1.7-1.9	$La(thd)_3/Al(acac)_3 + O_3$	325-400	0.3-0.5	[64]	
La_2O_3	1.6-1.9	$La[N(SiMe_3)_2]_3 + H_2O$	150-250	0.2-1.0	[65]	*
CaO	1.7-1.8	$Ca(Cp^{3i})_2 + H_2O$	205-300	0.4-1.2	[66]	*
MgO	1.7	$Mg_2(thd)_4 + H_2O_2$	325-525	0.4-2.0	[67]	*
Al_2O_3	1.6-1.7	$AlCl_3 + H_2O$	500	0.4	[31]	
		$Al(CH_3)_3 + H_2O$	100-500	1.1-1.3	[51, 68]	
		$Al(CH_3)_2Cl + H_2O$	200-500	0.4-0.8	[69]	
LaF_3	1.6	$La(thd)_3 + TiF_4$	225-350	1.8-5.2	[70]	*
YF_3	1.5-1.6	$Y(thd)_3 + TiF_4$	175-325	1.1-1.7		
ZnF_2	1.5	$Zn(O_2CCH_3)_2 + HF$	260-320	0.7-0.8	[32]	
SiO_2	1.4	$Si_2(NHC_2H_5)_6 + O_3$	150-300	0.8-1.1	[71]	
SrF_2	1.4	$Sr(thd)_2 + HF$	260-320	0.4-0.7	[32]	
CaF_2	1.4	$Ca(thd)_2 + HF$	300-400	0.2-0.4	[32]	
		$Ca(thd)_2 + TiF_4$	300-450	0.5-1.6	[72]	
MgF_2	1.3-1.4	$Mg(thd)_2 + TiF_4$	250-400	0.7-1.6	[73]	
		$Mg(thd)_2 + TaF_5$	225-400	0.4-1.1	[74]	

2.2 Optical coatings

Thin film interference filters have been used in many different applications in optics for a long time and their theory is very well known. The designing of filters has been done with computers already for more than twenty years and the optimization algorithms are quite mature. As computing power has increased rapidly during recent years, filters can now be designed using computer programs with little prior knowledge about thin films.

ALD was first introduced for optical coatings in 1996 by Riihelä et al. [31]. Since then, a few commercial optical coating applications have been introduced. ALD offers some unique properties, which make the technology viable for many special optical coating applications. ALD is still not seen as a general competitor for traditional optical coatings made by physical vapor deposition (PVD), as the PVD technology is very mature and less expensive in most optical coating applications for planar substrates.

The low growth rate of ALD can be compensated to some extent with large batches and optimized flows. Recent developments in spatial ALD methods might also find use in manufacturing of economical optical thin film filters.

2.3 Optical nanostructures and photonics

Photonic crystal structures can be fabricated by infiltrating colloidal materials by ALD and then etching the templating particles away. The first reported inverse opal structure was made by infiltrating colloidal silica particles using tungsten nitride (WN) ALD process by Rugge et al. in 2003 [75]. Fabrication and tuning of photonic crystals has since become the most examined application of ALD in photonics [75–97].

ALD is also a very promising technology for making and tuning photonic waveguides. ALD has been used to fabricate an active Er-doped Al_2O_3 waveguides, although net gain was not achieved [98]. ALD has also been applied in Erbium-doping of fiber soot [99]. The tunability can also be achieved by mixing thin layers of different materials, as Fig. 2.1 shows.

In this thesis, we propose narrowing of slot waveguides with ALD-TiO_2 [Publication I], estimate the effects of completely filling angled silicon slot waveguide structures [Publication II], measure the waveguiding proper-

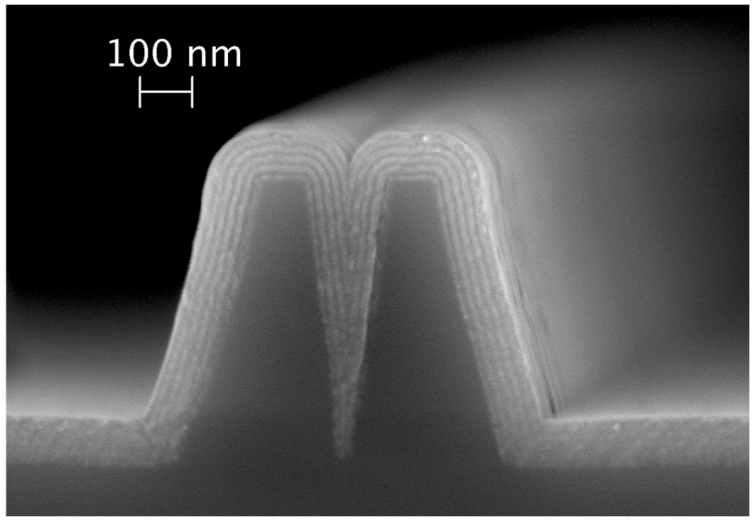

Figure 2.1. Scanning electron microscope (SEM) image of a slot structure fabricated on silicon and coated by an ALD nanolaminate. The used ALD processes were Al_2O_3 from TMA and water and TiO_2 from TiCl4 and water at 120 °C. The target film structure was 10 x (5 nm x Al_2O_3 + 5 nm x TiO_2).

ties of amorphous TiO_2 [Publication IV], and demonstrate reduction of losses in strip and slot waveguides by the same TiO_2 material [Publication III]. We also demonstrate ALD-TiO_2 in various grating structures [Publications IV,V,VI].

2.4 Industrial aspects

When ALD thin films are used in mass manufacturing, many more things than just the optical or electrical properties need to be taken into account. The physical and chemical durability of coatings has to be verified with careful testing. Also, the speed of processes and the cost of precursor materials become critical and the processes have to be optimized for the maximum speed and minimum material usage. Researchers often use chemicals that are not very viable in production environment. Ideal chemicals should be inexpensive, safe, easy to handle and have a relatively high vapor pressure at room temperature.

In research papers, the used processes are often run with long pulses to make sure that they are in the fully saturated regime. In industrial applications the length of pulses have to be optimized so that the process is the fastest possible with an acceptable yield. This sometimes results in processes that are not running in a fully saturated ALD-mode, but which

still provide good enough results.

One of the precursors is often non-volatile and thus does not form safety problems. For example, DI-water can be used in nearly all metal oxide processes and it is ultimately safe and almost free of cost. The volatile precursor chemicals tend to be more difficult to handle and more expensive. Some organic precursors also have relatively short shelf-time and tend to deteriorate. Trimethylaluminium (TMA, $Al_2(CH_3)_6$) and $TiCl_4$ are examples of good volatile precursor materials for industrial use. Although they are hazardous, the risks can be maintained with careful handling and the availability and the cost of the materials is very low. TMA, diethyl zinc (DEZ) and chlorides in general are quite preferable precursor materials for large area manufacturing because of their good availability and low cost.

Beta-diketonates are often used as ALD precursors in research papers, but they are often not very suitable to be used when a large amount of substrates is coated. Beta-diketonates are often only provided in small amounts for research use and the large scale production of the precursor material has to be organized for larger scale applications. Also, the growth rates of processes using complex organic ligands tend to be smaller than when using simpler ligands.

ALD also provides some benefits in the design and usability of deposition tools. As the repeatability is very good, ALD tools can be run in an open-loop without expensive in-situ monitoring and active controlling of the processes. If the machines are designed well, they can be run for years with little maintenance.

3. Photonic waveguides and gratings

This chapter gives an introduction to the theoretical background of waveguides and gratings, which is mostly based on the electromagnetic theory. The principles of the basic optics and optical devices have been discussed and explained in many good books and publications. Two such books are Born's and Wolf's '*Principles of optics: electromagnetic theory of propagation, interference and diffraction of light*' [100], and Yariv's and Yeh's more device oriented '*Photonics : optical electronics in modern communications*' [101], which have been used as the main sources in this chapter.

3.1 Electromagnetic theory and principles of waveguiding

3.1.1 Maxwell's equations

Everything in electromagnetic theory starts from Maxwell's equations:

$$\nabla \times \mathbf{E} + \frac{\partial}{\partial t}(\mu \mathbf{H}) = 0 \tag{3.1}$$

$$\nabla \times \mathbf{H} - \frac{\partial}{\partial t}(\varepsilon \mathbf{E}) = \mathbf{J} \tag{3.2}$$

$$\nabla \cdot (\varepsilon \mathbf{E}) = \rho \tag{3.3}$$

$$\nabla \cdot (\mu \mathbf{H}) = 0 \tag{3.4}$$

These laws were formulated by Scottish physicist James Clerk Maxwell, who published the finding in his work '*Treatise of Electricity and Magnetism*' in 1873. His theory states that all electric, magnetic, electromagnetic and optical phenomena are governed by the same fundamental laws of electromagnetism, which are written in above equations. In these equations, $\mathbf{E}$ is the electric field vector, and $\mathbf{H}$ is the magnetic field vector, which are often used to describe electromagnetic fields or optical waves.

The permittivity $\varepsilon(\mathbf{r})$, permeability $\mu(\mathbf{r})$, and the charge density $\rho(\mathbf{r})$ of the medium are scalars, when the medium is isotropic. **J** is the current density vector.

3.1.2 Polarization

The electric field of a plane wave can be represented by two orthogonal components, and the polarization state describes the relationship between amplitudes and phases of these two components. If the components have a phase difference of $\pi/2 + m\pi$, where m is an integer, the field is said to be circularly polarized (or elliptically polarized if the amplitudes are different). When the phase difference is a multiple of π, the field is linearly polarized. With the presence of a plane surface, the component that has the electric field perpendicular to the plane of incidence spanned by the wave vector and normal of the surface is called the transverse electric (TE) component, and the component which has the electric field parallel to the plane of incidence is the transverse magnetic (TM) component.

3.1.3 Refractive index

The refractive index is related to permittivity and permeability constants with relation:

$$n^2 = \frac{\varepsilon\mu}{\varepsilon_0\mu_0} = \varepsilon_r\mu_r, \tag{3.5}$$

where ε_r and μ_r are the relative permittivity and permeability, ε_0 is the permittivity of vacuum, and μ_0 is the permeability of vacuum. For most materials, $\mu_r \approx 1$ and thus $n^2 \approx \varepsilon_r$.

In lossy materials, the refractive index is a complex number. The complex part of the refractive index is often separated from the real part and called the extinction coefficient k.

Instead of scalar, permittivity can be represented by a tensor so that the refractive index is dependent on the direction of the electric field. In that case, the material is said to be birefringent.

For nonlinear optical materials, the refractive index is also dependent on the magnitude of the electric field. In this work, the most relevant nonlinear phenomenon is the Kerr effect, in which the refractive index depends on intensity according to

$$n = n_0 + \frac{3\chi^{(3)}}{8n_0}|E|^2 = n_0 + n_2 I, \tag{3.6}$$

where I is the intensity (the optical power per cross-sectional area), n_0 is

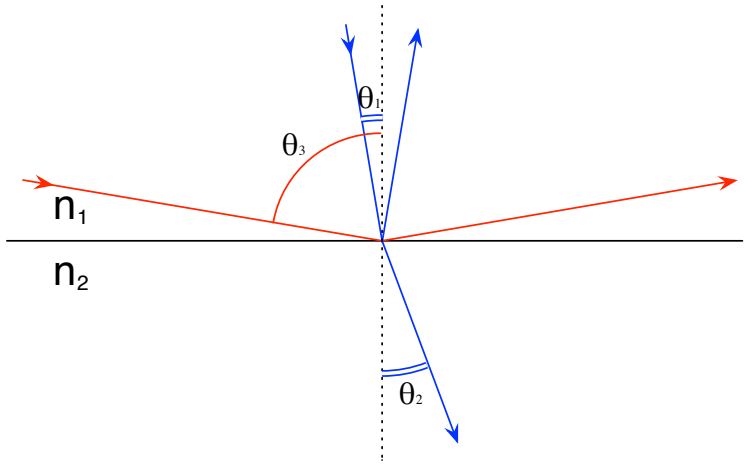

Figure 3.1. Light refraction at a dielectric interface when $n_1 > n_2$.

the refractive index of the material with low intensities, $\chi^{(3)}$ is the third order electric susceptibility of the medium, and n_2 the second-order nonlinear refractive index or Kerr index of the material.

3.1.4 Boundary conditions

Maxwell's equations have to be solved in parts for noncontinuous media. The wave equation is then solved separately for each part of the structure using a suitable set of boundary conditions. The boundary conditions can be deduced from Maxwell's equations using the Gauss and Stokes theorems [100].

3.1.5 Geometric optics treatment

Geometric optics may be used as well as electromagnetic theory to study wave propagation in homogenous dielectric materials. Using the boundary condition that the tangential components of **E** and **H** are continuous across any boundary, the Snell's law can be deduced:

$$n_1 \sin\theta_1 = n_2 \sin\theta_2, \tag{3.7}$$

where n_1 and n_2 are the refractive indices of the two media, and θ_1 and θ_2 are the angles to surface normal. If light is coming from the higher index medium and the angle is larger than the critical angle:

$$\theta_c = \arcsin(\frac{n_2}{n_1}), \tag{3.8}$$

total internal reflection occurs. Figure 3.1 shows a dielectric interface of materials having refractive indices n_1 and n_2. The angle for the red ray θ_3 is greater than θ_c and total internal reflection occurs. A part of light is reflected in the case of $\theta < \theta_c$ (blue ray in Fig. 3.1), and the rest of it is refracted to a larger angle.

3.1.6 Reflection at a boundary

The reflectance and transmittance of light at a boundary can be calculated with Fresnel's coefficients, which can also be derived from the boundary conditions of Maxwell's functions. The Fresnel's coefficients imply that the amplitude reflection at the interface is:

$$r = \frac{\eta_1 - \eta_2}{\eta_1 + \eta_2}, \tag{3.9}$$

where η_i ($i = 1, 2$) equals $n_i \cos\theta_i$ for TE-waves (s-polarisation) and $n_i / \cos\theta_i$ for TM waves (p-polarisation). The intensity reflectance is then

$$R = rr^* = \left| \frac{\eta_1 - \eta_2}{\eta_1 + \eta_2} \right|^2. \tag{3.10}$$

If there is no absorption in the materials (n is real), the transmittance through the boundary is:

$$T = 1 - R. \tag{3.11}$$

R and T in these equations are considered specular (i.e. measuring the direct rays as pictured in Fig. 3.1). Also total transmittance and total reflectance are sometimes considered, and those include also the scattered parts of light.

3.1.7 Reflection from a thin film stack

When light propagates a distance d from the surface, the phase change δ is:

$$\delta = \frac{2\pi n}{\lambda} d \cos\theta, \tag{3.12}$$

where n is the refractive index of the media and θ is the angle from the surface normal. This phase difference has to be taken into account, when reflections from different boundaries are calculated together.

A matrix notation can be deduced to help calculations when a stack of thin films is added between the cover boundary c and substrate s. A more rigorous deduction can be found in [102]. We denote the angle of incidence

by θ, and ψ and the effective index n_{eff} are the direction cosines in the positive quadrant multiplied by the refractive index:

$$\psi = n\cos\theta = \sqrt{n^2 - n_{\text{eff}}^2}, \tag{3.13}$$

$$n_{\text{eff}} = n\sin\theta. \tag{3.14}$$

We define the parameter γ as

$$\gamma = \begin{cases} n\cos\theta/z_0 & \text{for TE} \\ z_0\cos\theta/n & \text{for TM} \end{cases}, \tag{3.15}$$

where $z_0 = \sqrt{\mu_0/\varepsilon_0}$ is the impedance of free space. According to Maxwell's equations, the polarization-dependent field amplitudes U, V, and W are related by [102]

$$U = \frac{1}{ik\gamma\psi}\frac{\mathrm{d}V}{\mathrm{d}x}, \tag{3.16}$$

$$V = \frac{\gamma}{ik\psi}\frac{\mathrm{d}U}{\mathrm{d}x}, \tag{3.17}$$

$$W = \frac{n_{\text{eff}}\gamma}{\psi}U, \tag{3.18}$$

where $k = k_0 n$ is the wavenumber, $k_0 = 2\pi/\lambda$ is the vacuum wavenumber, and λ the (vacuum) wavelength of light.

We define a field-transfer Matrix M_j for transferring the field amplitudes U_j and V_j from point x_j to a second point x_{j-1}

$$\begin{pmatrix} U_{j-1} \\ V_{j-1} \end{pmatrix} = M_j \begin{pmatrix} U_j \\ V_j \end{pmatrix}. \tag{3.19}$$

We use the definition for the phase thickness δ_j (Eq. 3.12), with $d = x_j - x_{j-1}$ and the field-transfer matrix becomes [102]

$$M_j = \begin{pmatrix} \cos\delta_j & \frac{-i}{\gamma_j}\sin\delta_j \\ -i\gamma_j\sin\delta_j & \cos\delta_j \end{pmatrix}. \tag{3.20}$$

The reflected r_{cs} and transmitted t_{cs} amplitudes can be obtained from the matrix equation:

$$\begin{pmatrix} 1 + r_{cs} \\ \gamma_c(1 - r_{cs}) \end{pmatrix} = M \begin{pmatrix} 1 \\ \gamma_s \end{pmatrix} t_{cs}, \tag{3.21}$$

where M is the field-transfer matrix for all layers $M = M_1 M_2 \ldots M_J$. By solving the equations and denoting the elements of the 2×2 matrix M with m_{ij} (where i is the row, and j the column), we obtain:

$$r_{cs} = \frac{\gamma_c m_{11} + \gamma_c\gamma_s m_{12} - m_{21} - \gamma_s m_{22}}{\gamma_c m_{11} + \gamma_c\gamma_s m_{12} + m_{21} + \gamma_s m_{22}}, \tag{3.22}$$

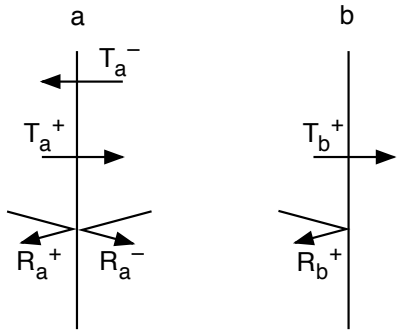

Figure 3.2. Naming conventions for R and T.

$$t_{cs} = \frac{2\gamma_c}{\gamma_c m_{11} + \gamma_c\gamma_s m_{12} + m_{21} + \gamma_s m_{22}}. \tag{3.23}$$

The intensity reflectance and transmittance are

$$R = |r_{cs}|^2, \tag{3.24}$$

$$T = \frac{\Re(\gamma_s)}{\Re(\gamma_c)}|t_{cs}|^2. \tag{3.25}$$

3.1.8 Incoherent reflection at two surfaces

The depth of the substrate is usually much greater than the coherence length of the light source. In that case, the incoherent reflection model is used and the intensities will be added instead of amplitudes. The total reflectance for light bouncing back and forth between the surfaces is given by:

$$\begin{aligned} R &= R_a^+ + T_a^+ R_b^+ T_a^- \left[1 + R_a^- R_b^+ + \left(R_a^- R_b^+\right)^2 + ...\right] \\ &= R_a^+ + \left[T_a^+ R_b^+ T_a^- \left(1 - R_a^- R_b^+\right)\right], \end{aligned} \tag{3.26}$$

for which the naming conventions are depicted in Fig. 3.2. T^+ and T^- are always identical and thus $T_a^+ = T_a^- = T_a$. Furthermore, if there is no absorption $R_a^+ = R_a^- = R_a$ and $R_a + T_a = 1$. Using these equations, R can be written as

$$R = \frac{R_a + R_b - 2R_aR_B}{1 - R_aR_b}. \tag{3.27}$$

Similarly, the transmittance without absorption is

$$T = \frac{T_aT_b}{1 - R_aR_b}. \tag{3.28}$$

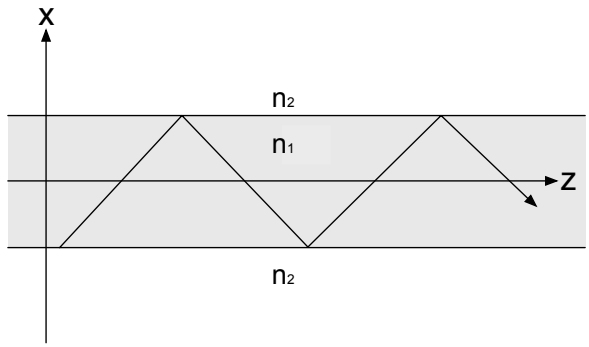

Figure 3.3. Dielectric slab waveguide, with the guiding layer of refractive index n_1 and the cladding of refractive index n_2.

3.2 Waveguides

3.2.1 Guided modes in slab waveguides

When the propagation happens in free space, diffraction will spread a beam of light with a finite cross section. In that case, lenses can be used at appropriate locations to focus and confine the propagation of beams. Optical fibers or dielectric slabs with higher refractive index core support confined electromagnetic propagation. These and other structures that support guided waves are called waveguides.

The simplest optical waveguide is a dielectric slab as shown in Fig. 3.3. It consists of a dielectric layer (with a refractive index n_1), called the core, sandwiched between two semi-infinite bounding media (with refractive indices n_2) called the cladding. To support guided modes, n_1 has to be greater than n_2.

If we consider the propagation of monochromatic radiation along the z axis in this case, we can write Maxwell's equations in the form [101]

$$\nabla \times \mathbf{H} = i\omega\varepsilon\mathbf{E}, \qquad \nabla \times \mathbf{E} = -i\omega\mu\mathbf{H}, \tag{3.29}$$

where ω is the angular frequency of the wave.

Since the structure is homogeneous along the z axis, the solutions can be taken as:

$$\begin{aligned} \mathbf{E}(x,t) &= \mathbf{E}_m(x) exp\left[i(\omega t - \beta_m z)\right], \\ \mathbf{H}(x,t) &= \mathbf{H}_m(x) exp\left[i(\omega t - \beta_m z)\right], \end{aligned} \tag{3.30}$$

where β_m is the propagation constant (the z component of the wavevec-

tors), $\mathbf{E}_m(x)$ and $\mathbf{H}_m(x)$ are wavefunctions of the guided modes, with subscript m being the mode number (an integer). If there is only a single bound mode solution to the equation, the waveguide is called single-moded. If we assume a layered dielectric structure of homogeneous and isotropic materials, the wave equation for the transverse electric (TE) field can be obtained by eliminating $\mathbf{H}$ from Eq. 3.29:

$$\frac{\partial^2}{\partial x^2}\mathbf{E}_m(x) + \left[k_0^2 n^2(r) - \beta^2\right]\mathbf{E}_m(x) = 0, \tag{3.31}$$

where $k_0 = \omega/c$ is the wavenumber in vacuum. The effective index n_{eff} of the mode is β/k_0. For the TM waves, the electric field is not continuous at the dielectric interfaces and we have to use a similar equation solved be eliminating the $\mathbf{E}$ instead of $\mathbf{H}$. The propagating mode for each polarization has then to be solved separately in each segment of the structure and then the tangential components of the field vectors need to be matched at each interface.

The same matrix formalism we used in Section 3.1.7 may be used to solve the modes of slab waveguides. Using the previous definitions, the fields at the stack boundaries have to satisfy a condition

$$\begin{pmatrix} U_c \\ V_c \end{pmatrix} = M \begin{pmatrix} U_s \\ V_s \end{pmatrix}, \tag{3.32}$$

where the c subscript denotes the cover and s the substrate, and M is the field-transfer matrix for all layers $M = M_1 M_2 \ldots M_J$.

The radiation condition requires negative-going waves in the cover and positive-going waves in the substrate so for the bound modes the equation becomes [102]

$$\begin{pmatrix} 1 \\ -\gamma_c \end{pmatrix} U_c = M \begin{pmatrix} 1 \\ \gamma_s \end{pmatrix} U_s. \tag{3.33}$$

By solving these equations, we can define a modal-dispersion function χ_M

$$\chi_M(n_{\text{eff}}) \equiv \gamma_c m_{11} + \gamma_c \gamma_s m_{12} + m_{21} + \gamma_s m_{22} = 0, \tag{3.34}$$

from which the effective indices of the modes can be solved. For bound modes the modal function χ_M is imaginary and there exists only a discrete set of roots that satisfy the modal condition.

The propagation can also be studied with geometrical optical treatment by looking at the total internal reflection and the phase changes. Even though total internal reflection is a necessary condition, not all rays trapped by the total internal reflection constitute a mode. The totally reflecting ray will only become a mode when the extra transverse phase shift

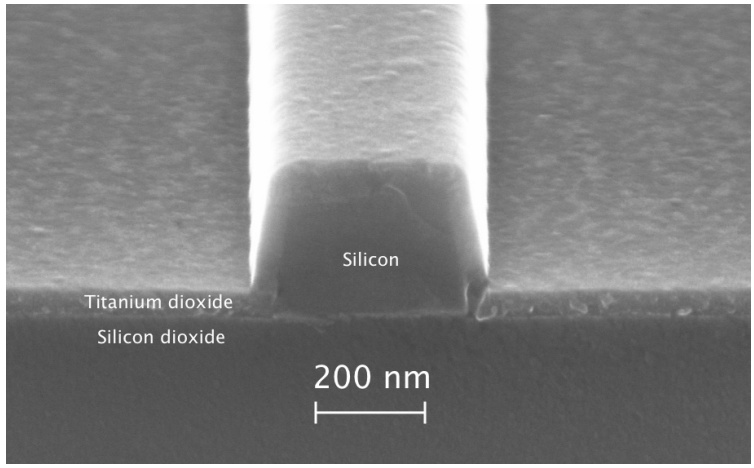

Figure 3.4. Scanning electron microscope (SEM) image of a cross-section of a silicon strip waveguide that is ALD-coated with a 50 nm thick layer of TiO_2.

between the reflections is an integral multiple of 2π so that there is a constructive interference.

3.2.2 Strip waveguides

Strip waveguides are rectangular waveguides of high-index material surrounded by lower index materials. An example of a silicon strip waveguide ALD-coated with approximately 50 nm of titanium dioxide (TiO_2) is shown in Fig. 3.4. This geometry offers good confinement in both vertical and horizontal directions.

The propagation modes for strip waveguide geometries are solved from Maxwell's equations numerically. The dimensions can be adjusted to get suitable dispersion and other properties. For a high-index contrast strip waveguide with nanoscale dimensions, the evanescent field (which extends from the waveguide core boundary into the surrounding cladding with an exponential decay) can be relatively strong at the waveguide surfaces. The strong field can be used with nonlinear cladding material in nonlinear optical applications [103] or in waveguide sensors [104].

Strip waveguides made on silicon-on-insulator (SOI) platform are widely used in many kinds of silicon photonics applications.

3.2.3 Slot waveguides

Slot waveguides were proposed in 2004 by Almeida et al. to create a waveguide that confines light in low refractive index material, but that

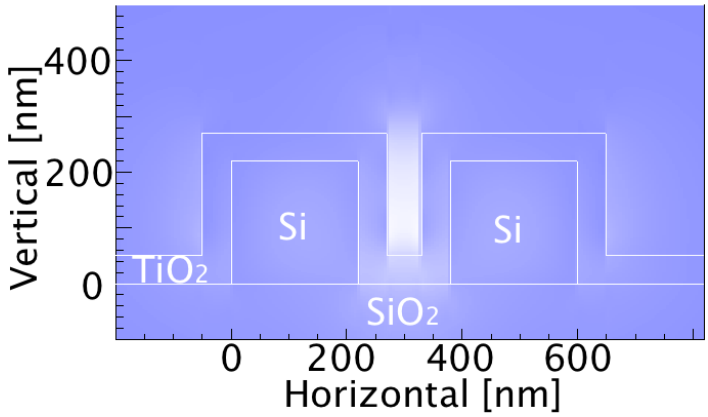

Figure 3.5. Calculated transverse electric field (E_x) mode profile of a silicon slot waveguide ALD-coated with a 50 nm thick layer of TiO_2.

is still based on total internal reflection [105]. The device was also experimentally demonstrated later the same year [106]. With slot waveguides, more electrical field can be confined into the slot region. As the slot can be filled with suitable low refractive index materials, this makes silicon photonics platform even more interesting for nonlinear optical [103] and sensing [107–109] applications.

As the slot waveguide devices on silicon require very small dimensions, the fabrication is quite problematic. In Publication I we proposed to use ALD-TiO_2 to narrow down silicon slot waveguide structures to better control the slot width. We also simulated how ALD materials would work to completely fill the slot waveguides in Publication II. We demonstrated that the surface smoothening feature of ALD can be used to reduce losses in silicon strip and slot waveguides in Publication IV. Figure 3.5 shows a mode profile of a silicon slot waveguide ALD-coated with TiO_2, which demonstrates the guiding of light in the low refractive index air slot.

3.2.4 Computational methods for solving waveguide modes

The waveguide modes for geometries more complex than slab waveguides can be solved from Maxwell's equations using approximative or numerical methods such as the effective index method, the finite-element method (FEM) [110], the finite difference method (FDM) [111] or as in this thesis film-mode matching method (FMM) [112]. Each technique has its strengths and different methods are used for different problems. For ex-

ample, the FEM method is often used for complex waveguide geometries, as in FEM the field region is divided into an irregular grid of elements of various shapes like triangles or rectangles. In many cases it may be useful to first try fast approximate methods to build intuition and narrow the parameter range, and then refine calculations using more advanced and accurate numerical approaches.

In this thesis, the FMM solver of the FIMMWAVE software was used [113]. In FMM, the waveguide is divided into vertical slices, which are uniform laterally, but composed of a number of vertical layers [113]. A 2-dimensional mode is built up from the 1-dimensional TE and TM modes for each slice. The method is theoretically exact for an infinite number of 1-dimensional modes. The modeled area may have either perfect metallic or magnetic walls, or periodic boundary conditions. FMM works well for solving modes of rectangular waveguides.

3.2.5 Surface roughness and loss in waveguides

In the case of silicon-on-insulator (SOI) platform, the waveguide losses are mainly due to sidewall surface roughness, and also due to leakage through the buried oxide into the silicon substrate if the optical field is not sufficiently guided. Furthermore, the surface states at the uncovered waveguide boundaries can lead to excess absorption.

Surface roughness leads to scattering losses, and a detailed theoretical description backed up with experiments has been published for the case of high index-contrast three-dimensional strip waveguides by Poulton et al. [114], where intuitively understandable guidelines were given for fabricating low-loss waveguides.

For the simple case of two-dimensional slab waveguides as depicted in Fig. 3.3, a coupled-mode formalism was developed [115]. The theory is also instructive for other waveguide geometries to see the tendency from the closed-form relation for the loss coefficient α (unit dB/cm) [115],

$$\alpha = 4.34\ \varphi^2(d)\big(n_1^2 - n_2^2\big)^2 \frac{k_0^3}{4\pi n_1} \int_0^{\pi} \check{R}(\beta - n_2 k_0 \cos\theta)\,\mathrm{d}\theta. \tag{3.35}$$

Here, $\varphi(d)$ is the normalized modal field ($\int_{-\infty}^{+\infty} \varphi^2(x)\,\mathrm{d}x = 1$) at the core-cladding boundary $x = \pm d/2$ of the symmetric slab waveguide having a width d. Core and cladding refractive indices are denoted as n_1 and n_2, respectively, $k_0 = \omega/c$ is the free-space wavenumber for an angular frequency ω and the vacuum speed of light c, the so-called spatial power spectrum $\check{R}(\theta)$ is the Fourier transform of the surface roughness autocor-

relation function $R(u)$, and β is the modal propagation constant. This formula has been used in many publications assuming an exponential autocorrelation function $R(u) = \sigma^2 e^{-|u|/L_c}$ and thereby explaining measured losses in Si waveguides [116–118].

3.3 Gratings

Gratings are periodic optical structures with the periodicity in the wavelength scale. Generally, a grating is an optical structure whose dielectric and permeability constants (tensors) are periodic functions of position:

$$\begin{aligned} \varepsilon(\mathbf{x}) = \varepsilon(\mathbf{x}+\mathbf{a}) = \varepsilon_0 n^2(\mathbf{x}+\mathbf{a}), \\ \mu(\mathbf{x}) = \mu(\mathbf{x}+\mathbf{a}), \end{aligned} \tag{3.36}$$

where $\mathbf{a} = \mathbf{i}d_x + \mathbf{j}d_y$ is any arbitrary lattice vector. The Eqs. 3.29 must remain the same if we substitute $\mathbf{x}$ for $\mathbf{x}+\mathbf{a}$. The translational symmetry requires that the normal modes of propagation are:

$$\begin{aligned} \mathbf{E} = \mathbf{E}_\mathbf{K}(\mathbf{x}) \exp\left(-i\mathbf{K}\cdot\mathbf{x}\right), \\ \mathbf{H} = \mathbf{H}_\mathbf{K}(\mathbf{x}) \exp\left(-i\mathbf{K}\cdot\mathbf{x}\right), \end{aligned} \tag{3.37}$$

where both $\mathbf{E}_\mathbf{K}$ and $\mathbf{H}_\mathbf{K}$ are periodic functions of $\mathbf{x}$:

$$\begin{aligned} \mathbf{E}_\mathbf{K}(\mathbf{x}) = \mathbf{E}_\mathbf{K}(\mathbf{x}+\mathbf{a}), \\ \mathbf{H}_\mathbf{K}(\mathbf{x}) = \mathbf{H}_\mathbf{K}(\mathbf{x}+\mathbf{a}). \end{aligned} \tag{3.38}$$

This is known as Floquet-Bloch theorem and it states that the fields are periodic within $\mathbf{x}$ and $\mathbf{x}+\mathbf{a}$, apart from the phase factor $\exp\left(-i\mathbf{K}\cdot\mathbf{x}\right)$. The functions $\mathbf{E}_\mathbf{K}$ and $\mathbf{H}_\mathbf{K}$ depend on the Bloch wavevector $\mathbf{K}$.

Let us consider the case of a 2-dimensional crossed grating as illustrated in Fig. 3.6, with refractive indices n_I in the region I and n_III in region III. When the grating is illuminated with an incident plane wave $\mathbf{E_0}(x, y, z; \omega)$, a discrete set of reflected and transmitted plane waves are generated as the field in regions I and III is pseudo-periodic and follows the Floquet-Bloch theorem (Eq. 3.37).

Let us define the k_{x0}, k_{y0}, and k_{z00} as the x, y, and z components of the wave vector of the incident light. From the Floquet-Bloch condition it follows that the wave vector components of the reflected and transmitted plane waves can only have discrete values:

$$k_{xm} = k_{x0} + \frac{2\pi m}{d_x}, \tag{3.39}$$

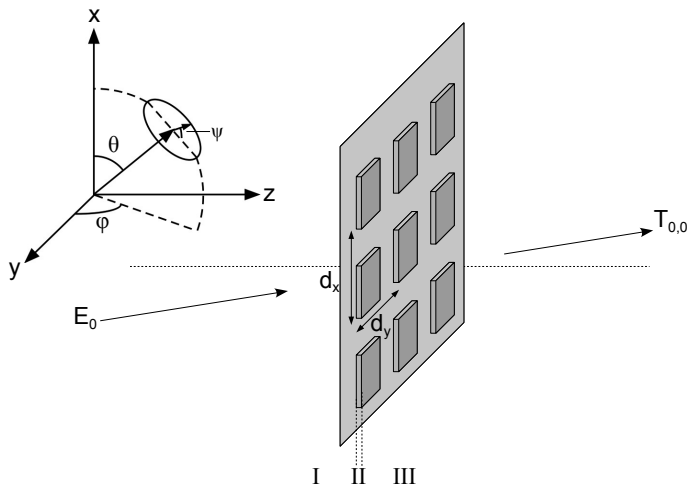

Figure 3.6. Geometry of a 2-dimensional grating.

$$k_{yn} = k_{y0} + \frac{2\pi n}{d_y}, \tag{3.40}$$

$$k_{zmn} = \sqrt{(k_0 n_i)^2 + k_{xm}^2 - k_{yn}^2}, \tag{3.41}$$

where m and n are integers corresponding to the respective diffraction orders, $k_{x0} = k_0 n_i \sin\theta\cos\varphi$, $k_{y0} = k_0 n_i \sin\theta\sin\varphi$, $k_{z00} = n_i k_0 \cos\theta$, $k_0 = 2\pi/\lambda$ is the vacuum wave number, and n_i is either n_{I} or n_{III} depending on the region.

The discrete set of reflected fields (region I) and transmitted fields (region III) can be formulated using so-called Rayleigh expansions:

$$\mathbf{E}_{\mathrm{I}}(x,y,z;\omega) = \sum_{m=-\infty}^{\infty}\sum_{n=-\infty}^{\infty} \mathbf{r}_{mn} \exp\left[i(k_{xm} + k_{yn} + k_{zmn}^{-} z)\right], \tag{3.42}$$

$$\mathbf{E}_{\mathrm{III}}(x,y,z;\omega) = \sum_{m=-\infty}^{\infty}\sum_{n=-\infty}^{\infty} \mathbf{t}_{mn} \exp\left[i(k_{xm} + k_{yn} + k_{zmn}^{+}(z-h))\right]. \tag{3.43}$$

If we denote the angles of diffracted plane waves by θ_{mn} and take into account that the plane waves must fulfill a condition $k_{zmn} = k_0 n_i \cos\theta_{mn}$, we can write the grating equation for transmitted diffraction orders as

$$k_0^2 n_{\mathrm{III}}^2 \sin^2\theta_{mn} = (k_0 n_{\mathrm{I}} \sin\theta\cos\varphi + 2\pi m/d_x)^2 + (k_0 n_{\mathrm{I}} \sin\theta\sin\varphi + 2\pi n/d_y)^2, \tag{3.44}$$

and for the reflected diffraction orders as

$$k_0^2 n_{\mathrm{I}}^2 \sin^2\theta_{mn} = (k_0 n_{\mathrm{I}} \sin\theta\cos\varphi + 2\pi m/d_x)^2 + (k_0 n_{\mathrm{I}} \sin\theta\sin\varphi + 2\pi n/d_y)^2. \tag{3.45}$$

The grating equations for one-dimensional grating are obtained, when $\varphi = 0$, $d_x = d$, and $d_y \to \infty$.

The diffraction efficiencies for the transmitted and reflected diffraction orders are obtained from

$$\eta_{tmn} = \Re\left\{k^{+}_{zmn}/k^{+}_{z00}\right\}|\mathbf{t}_{mn}|^2, \tag{3.46}$$

$$\eta_{rmn} = \Re\left\{k^{-}_{zmn}/k^{-}_{z00}\right\}|\mathbf{r}_{mn}|^2, \tag{3.47}$$

where $\Re\left\{k^{+}_{zmn}/k^{+}_{z00}\right\}$ and $\Re\left\{k^{-}_{zmn}/k^{-}_{z00}\right\}$ are scaling factors that arise from the energy conservation as the cross-section of the incident and diffracted beams change when their propagation angles change.

3.3.1 Fourier modal method

The complex amplitudes of the reflected and transmitted diffraction orders (Eqs. 3.42 and 3.43) can be solved using various numerical methods, such as Rayleigh, Integral [119], and Coordinate transform [120] methods. The principle of the Fourier modal method [121–123] is to slice the permittivity profile of the grating (region II in Fig. 3.6) and to express the field inside the modulated region and the sliced permittivity profile as a Fourier series. The slices do not have to be equally spaced and together they form a periodic, piece-wise-constant medium. The Fourier coefficients as well as the wave vector z-components of the modes are solved numerically from eigenvalue equations, and the fields are matched at each boundary separately.

The accuracy of the Fourier modal method depends on the number of diffraction orders taken into calculations. For a converged result, all the propagation modes and a sufficient number of evanescent modes must be included. In the case of metallic gratings, a larger number of modes have to be taken into account.

3.3.2 Resonant waveguide gratings

Resonant waveguide gratings (RWG), also called guided mode resonance filters (GMRF), are a special case of gratings where the diffracted modes are coupled to the waveguiding modes of the grating and back [124, 125]. In RWGs, 100% switching of optical energy between reflected and transmitted waves occurs over small parameter ranges. Potential uses for these elements include filters, sensors, pulse-shapers, second-harmonic genera-

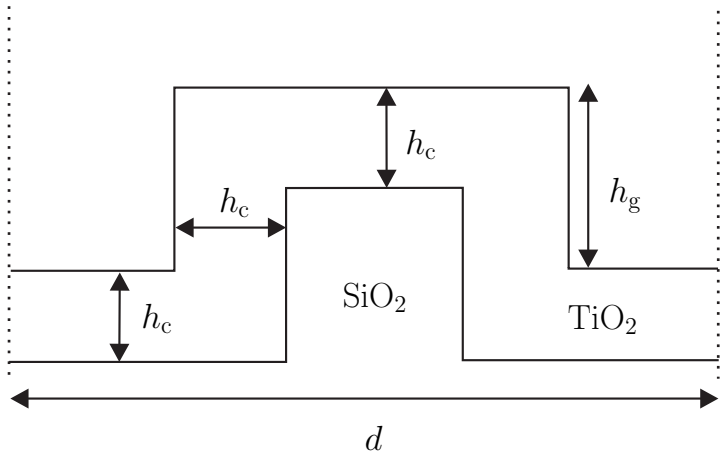

Figure 3.7. Schematic of an RWG grating where h_c is the thickness of the TiO_2 coating, h_g is the height of the grating, and d is the period of the grating. The substrate material is SiO2. [From Publication VI]

tion, and field enhancement of fluorescence [125–128]. RWG biosensors have also been used in living cell sensing [129].

The guided-mode resonance may also yield an almost total absorption of one polarization component and greatly enhance the absorption in localized surface plasmon resonance [Publication V]. In Publication VI we have shown that by using high quality ALD-TiO_2 as the waveguiding material in the RWG, a wider bandwidth in visible wavelengths for one of the polarizations is also possible. The schematic of one period of such RWG is shown in Fig. 3.7.

4. Methods

4.1 Patterning of optical nanostructures

Depending on the application and its requirements, different nanofabrication methods are preferred. Typical technologies include different lithography methods, including photolithography, electron beam lithography (EBL), and nano-imprint lithography, for inorganic structures and injection molding and UV replication for polymers. Other methods include direct holographic patterning of sinusoidal surface relief gratings, which is covered in the next section. A more complete overview of different fabrication methods can be found in [130].

Lithographic patterning is done in a few consequent steps. First a resist is applied on a clean substrate by spin coating. A liquid solution of the desired resist is dispensed on the wafer, and the wafer is spun rapidly to produce a uniform, typically 500–2500 nm thick, layer. In electron beam lithography, the used resist is typically polymethyl methacrylate (PMMA). The resist is then exposed to either a scanning beam of electrons (in EBL) or photons through a photomask (in photolithography).

The resolution of the lithography is dependent on the wavelength of the radiation, and thus shorter wavelengths are preferred. The wavelength of electrons is in the picometer range, and the accuracy is limited more by the accuracy of the beam steering. Commonly used state-of-the-art photolithography uses deep ultraviolet (DUV) excimer lasers with 193 nm or 248 nm wavelengths, which provide a resolution of down to 50 nm. The photomasks for DUV lithography are usually done by EBL.

After the exposure, the resist is developed with suitable chemicals and heating procedures to remove either the exposed (positive resist) or unexposed (negative resist) areas. The development phase may include multiple chemicals and baking steps, and after them we have a durable solidi-

fied resist that can be used in etching.

The etching may be done in a liquid etchant (wet etching) or with plasma gases (dry etching). Dry etching usually provides better accuracy and low-defectivity processes have been developed to transfer even the smallest features of the photoresist to the underlying substrate.

Silicon waveguides are usually made on the silicon-on-insulator (SOI) platform. SOI wafers are special silicon wafers, which have a thin (typically 200–300 nm) single crystalline silicon device layer on top of a thicker buried oxide (BOX) layer of silicon dioxide (typically 2–3 μm thick). The waveguides used in Publication III were fabricated on SOI wafers with a 220 nm device layer and a 2 μm BOX layer using 193 nm DUV lithography.

4.2 Direct holographic patterning of azobenzene polymers

The light-induced motions of the azobenzene molecules can be used to inscribe surface-relief structures into the material system. The surface relief gratings are fabricated by first spin coating the substrate with the azobenzene polymer complex, e.g. that consists of 4-dimethylamino-4'-hydroxyazobenzene (OH-DMA) azo dye and poly(4-vinyl pyridine) (P4VP) polymer (i.e. P4VP(OH-DMA)$_x$), and then exposing it to an interference pattern made using an extended laser beam of a suitable wavelength [131]. A detailed study of the azobenzene polymer complexes can be found in [132].

To write the surface-relief grating, an argon-ion laser with an output wavelength of 488 nm was used. The beam was expanded with a telescope and cropped with an adjustable pinhole to have a 0.5 cm diameter and $\sim$60 mW of output power ($\sim$300 mW/cm^2). A $\lambda/4$–plate was used before the cropping to translate the linearly polarized beam to a circularly polarized one. The interference pattern was formed using a Lloyd's mirror setup, so that the left half-circle of the beam interfered with the right half-circle. An exposure time of 20 minutes was used to ensure that the writing process was completely saturated.

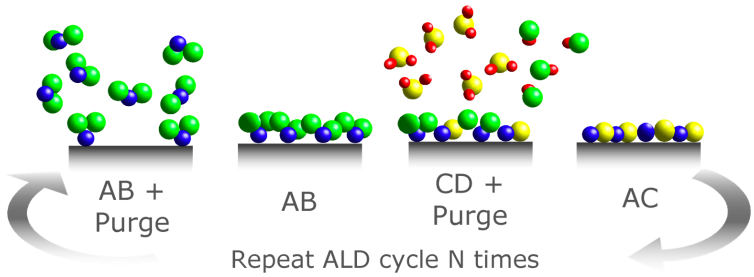

Figure 4.1. The steps of an ALD cycle. The final thin film is a combination of parts of the precursor materials and other reaction products are purged away. (Picture courtesy of Beneq Oy)

4.3 ALD processing

In this section, the chemistry of ALD processes is explained only briefly, as there are many general reviews on ALD (e.g. [133–139]), which explain the details more completely. There are also reviews about ALD for synthesis and surface engineering of nanostructures by Knez et al. [140] and about applications of ALD to nanofabrication by Kim et al. [141]. The overview of optical applications of ALD was covered in Chapter 2.

ALD is a gas phase vapor process that typically operates in vacuum. Substrates are placed in a reaction chamber where temperature, pressure, and other parameters are adjusted according to the process chemistry and wanted film properties. Two chemicals are then supplied sequentially to a deposition zone and they form a thin film of material as they react with each other on the surface. ALD is thus based on sequential self-terminating gas–solid reactions.

The ALD process cycle can be divided into four steps:

1. The substrate is exposed to the first precursor, which forms a saturated layer by reacting with the surface groups.

2. The excess precursor and reaction by-products are purged out.

3. The surface groups formed by the first precursor are exposed to the second precursor, which also forms a saturated layer.

4. The excess precursor and reaction by-products are purged out.

The steps of an ALD cycle are also shown in Figure 4.1. As precursors are pulsed to the reaction chamber separately, the reaction happens only on the surface. First, a dose of a precursor material is pulsed to the reac-

tion chamber and it reacts with the surface. The excess vapor is purged with a nitrogen pulse, before the second precursor is pulsed to the chamber. The second precursor vapor then reacts with the first precursor on the surface and a partial layer of the desired film is formed. Finally, the excess precursor vapor and by-products are purged with nitrogen before the cycle begins again with the first precursor. As a result, there is a binary-type growth of films and the thickness can be controlled very accurately by varying the amount of cycles.

The speed of growth is usually counted in growth rate per cycle. Self-limited growth rates vary from less than 0.1 nm/cycle of some nitrides to 1-12 nm/cycle of SiO_2:Al [142]. Usually, only a fraction of a monolayer is formed with a single cycle, because the precursor ligands take larger space on the surface than the reaction product. Also, the length of the used precursor and purge pulses often affect the actual growth rate a little, as the saturation happens asymptotically.

A large range of materials can be grown by ALD. The periodic table including the possible materials can be found from Puurunen's review [12]. The principle of ALD is simple but in reality the ALD growth is a complex mixture of interaction of chemicals, temperature, time, flow and coating tool technical construction details. Results achieved with one deposition platform are not always transferrable to other deposition tools.

4.3.1 Effect of temperature on ALD process

ALD processes usually work well and the growth rate is constant in a limited temperature range, which is called the "ALD window". Below the ALD window, the growth rate can be either higher because of precursor condensation or lower due to insufficient reactivity. And above the ALD temperature window, the growth rate can be higher due to precursor decomposition or lower because of precursor desorption. Sometimes the growth rate is dependent on the number of available reactive sites or on the film density.

4.3.2 Variants of ALD

In addition to the usual thermal ALD method, there are many other variants of ALD. In plasma-enhanced ALD (PEALD), plasma radicals are used instead of normal gases to get additional energy to the process. Typically oxygen (for oxides), nitrogen or ammonia (for nitrides), or hydrogen

plasma (for metals) is used. Plasma can be either direct or remote, and either capacitively or inductively coupled. In radical-enhanced ALD (RE-ALD), a remote plasma source is placed far from the substrate so that the electrons and ions from the plasma are not surviving to the substrate region.

A spatial ALD has also gained lot of interest recently. In the spatial ALD, the precursors are delivered to the surfaces by moving the substrate through different gas zones or by moving an ALD head (with the separate precursor gas zones) above the substrate. Special attention has to be paid to keep the different precursor gases from reacting in the gas phase by carefully designed inert gas barriers.

4.3.3 Titanium tetrachloride / water process

This thesis focuses on titanium dioxide (TiO_2) films made by titanium tetrachloride ($TiCl_4$) / water (H_2O) ALD process. To achieve good optical properties, we have chosen 120 °C temperature for most of our TiO_2 studies. The chemistry of the process and the effect of different deposition parameters has been studied before [19].

The basic reaction between $TiCl_4$ and H_2O is:

$$TiCl_4 + 2\ H_2O \longrightarrow TiO_2 + 4\ HCl. \tag{4.1}$$

The actual surface reactions are a complicated mixture of different reactions between $TiCl_4$ and the OH-surface groups, which form –O–$TiCl_n$ or other Cl-containing groups, and for the second part H_2O reacting with the Cl-containing groups and forming OH-groups [17, 143]. The films grown in a cross-flow type reactor tend to have some thickness profile along the flow direction. This has been suggested to be due to the HCl by-product reacting again either with the OH-groups, Cl-groups or both on the surface and thus hindering the growth downstream [17]. In our experiments at the 120 °C, we typically see a thicker stripe of film on the input side of the reaction chamber, but further downstream the non-uniformity is below $\pm$ 1%. The used ALD tool was a Beneq TFS 500 with a reactor chamber designed for 200 mm wafers.

4.3.4 Conformal growth mode of ALD

Because of the surface reactions, ALD has a constant-rate contour growth mode, i.e., the films grow along the surface normal at a constant rate.

This has been used to grow nano- and microlens arrays [144] and to fill and planarize optical gratings [15]. We have shown in Publications I and III that the growth mode can be used to narrow silicon slot waveguides.

The growth mode can also be used to reduce surface roughness and thus waveguide losses as demonstrated in Publication III. The ALD growth on a rough surface can be simulated using a model, based on solving a partial-differential equation. The conformal change of an initial surface height geometry $h(x,0)$ due to the cyclic growth of ALD monolayers is described as a function of position x and cycle number τ. Because of the large number of ALD monolayers per the final layer, the cycle number τ can be regarded as a continuous "time" variable. We write

$$\frac{\partial h(x,\tau)}{\partial \tau} = v\sqrt{1+\left(\frac{\partial h(x,\tau)}{\partial x}\right)^2}, \tag{4.2}$$

where the quantity v is the ALD growth rate, and $v\,\tau$ is the thickness of the final layer. The model is based on having the growth rate directly proportional to the surface area. To visualize the ALD growth of materials like amorphous Al_2O_3 or TiO_2, a typical growth rate of $v = 0.1$ nm/cycle was chosen.

The Eq. (4.2) solved with a finite difference scheme gives

$$\begin{aligned} h_{i,j+1} = h_{i,j} + \tfrac{\Delta h}{2}\left[\sqrt{1+\left(\tfrac{h_{i,j}-h_{i-1,j}}{\Delta x}\right)^2} + \sqrt{1+\left(\tfrac{h_{i+1,j}-h_{i,j}}{\Delta x}\right)^2}\right] \\ + \tfrac{\Delta h^2}{2\Delta x^2}\left[h_{i+1,j} - 2h_{i,j} + h_{i-1,j}\right], \end{aligned} \tag{4.3}$$

where $\Delta h = 0.1$ nm is the growth rate/cycle, Δx is the fixed position step (0.1 nm was used as well), j is the cycle number, and i is the position.

For the surface to be covered, we assumed an exponentially distributed initial height profile $h(x,0)$ with an autocorrelation length $L_c = 50$ nm and a root-mean-square (RMS) roughness of $\sigma = 5$ nm. A 20 μm wide calculation window with periodical boundary conditions (i.e. $h_{0,x} = h_{N+1,x}$ and $h_{-1,x} = h_{N,x}$, where N is the furthest position) was used. The smoothening of a surface roughness profile as a function of thickness solved using Eq. 4.3 is shown in Fig. 4.2. The previously mentioned parameters were used, but only 300 nm wide part of the profile is shown.

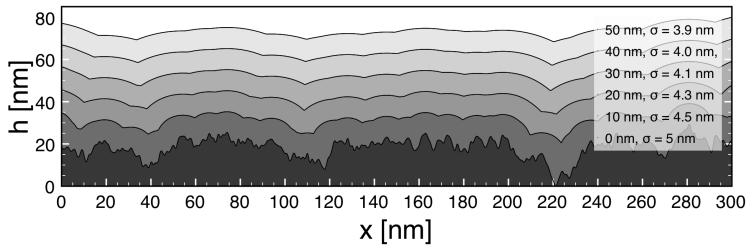

Figure 4.2. Simulation of the ALD growth on a rough surface. The initial surface roughness is exponentially distributed having a correlation length of $L_c = 15\,\mathrm{nm}$ and a root-mean-square (RMS) roughness of $\sigma = 5\,\mathrm{nm}$. The height profiles $h(x)$ and the RMS roughnesses σ are shown for various thicknesses $(0, 10, \ldots, 50)\,\mathrm{nm}$ of the deposited layer in steps of $10\,\mathrm{nm}$.

4.4 Characterization methods

4.4.1 Spectrophotometry

In spectrophotometry, the light transmittance through a sample or the reflectance from a sample are measured as a function of wavelength. A spectrophotometer usually consists of a light source, a monochromator, and a photodetector. The monochromator is usually of scanning type, but can be fixed as well if the photodetector is movable. Also, an array of photodetectors (such as charge coupled devices (CCD) or photodiodes) are sometimes used with a fixed monochromator. The sample can be placed either before or after the monochromator. The commercially available spectrophotometers cover partly or fully the wavelength range 200. . . 2500 nm.

Dual beam spectrophotometers compare light propagating through two different paths, and the sample is placed in the other path. Dual beams provide more stability against variations in the light source spectrum, which can vary over time. In single beam measurements, the spectrum of the light source is assumed to be the same when the reference spectrum is taken and after the sample is inserted.

Spectrophotometry can be used to accurately determine the thickness of thin films, if the film is thick enough to result in an interference peak within the measured wavelength range. We use the equations in Sections 3.1.7 and 3.1.8 to determine the transmittance of a given substrate-film system. The refractive index profile is chosen with a suitable refractive index model like Cauchy model:

$$n(\lambda) = A + \frac{B}{\lambda^2} + \frac{C}{\lambda^4}, \tag{4.4}$$

where A, B, and C are the Cauchy constants and λ is the wavelength. The Cauchy model is only valid above the bandgap of a dielectric material and in the visible range. Sellmeier's equation can also be used to get a more accurate fit at ultraviolet and infrared wavelengths:

$$n(\lambda) = \sqrt{1 + \frac{A_1\lambda^2}{\lambda^2 - B_1} + \frac{A_2\lambda^2}{\lambda^2 - B_2} + \frac{A_3\lambda^2}{\lambda^2 - B_3}}, \tag{4.5}$$

where $A_{1,2,3}$, and $B_{1,2,3}$ are the Sellmeier coefficients. Usually, it is enough to have just the first A_1 and B_1 parameters to get good accuracy.

The parameters affecting the calculated transmittance are varied using a suitable algorithm (e.g. Levenberg-Marquardt algorithm [145]) to minimize the difference between the calculated and measured transmittance spectra. A reasonably good starting guess has to be given to the algorithm, otherwise it may converge to a local minimum far away from the real parameters. In reflectometry, the reflectance is determined instead of transmittance and corresponding equations are then used.

4.4.2 Ellipsometry

Ellipsometry is also a powerful technique to determine the complex refractive index of a thin film. As its name suggests, an ellipsometer measures the ellipticity of the polarization state of light reflected from a surface. The ellipsometer parameters are the amplitude ratio $\tan(\Psi)$ and the phase shift Δ, which are defined by the complex reflectance ratio ρ:

$$\rho = \frac{r_{TM}}{r_{TE}} = \tan(\Psi)e^{i\Delta}, \tag{4.6}$$

where r_{TM} and r_{TE} are the complex Fresnel coefficients (see Eq. 3.9). As the difference between different polarizations is used instead of the actual reflectance, there is no need for a good reflectance reference as in the case of reflectometry.

The refractive index has to be solved again in a similar way than in the spectrophotometer case using a suitable refractive index model and choosing the best fit of thickness and model parameters. This time we just have to solve the $\tan(\Psi)$ and Δ parameters as a function of wavelength, and not the transmittance and reflectance.

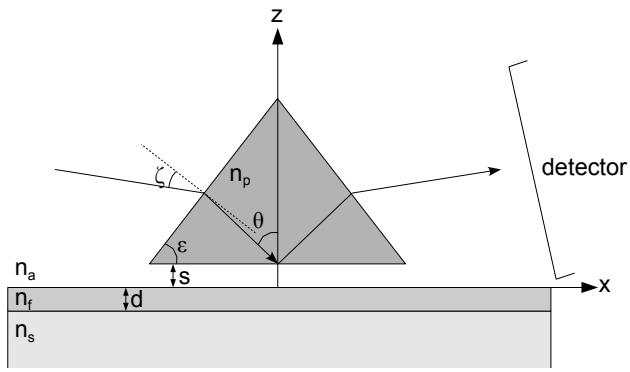

Figure 4.3. Schematic of the prism coupling setup.

4.4.3 Prism coupling method

The prism coupling method can be used to measure the thickness, and the refractive index properties of slab waveguides [146, 147]. Figure 4.3 shows the schematic of a prism coupling setup. In prism coupling, the propagating modes of the slab waveguide are measured by monitoring the coupling of a monochromatic beam of light from a laser source to a thin film on a substrate. The actual measured parameter is the incident angle ζ, from which the effective index can be solved using [147]

$$n_{\text{eff}} = \cos\varepsilon \ \sin\zeta + \sin\varepsilon\sqrt{n_p^2 - \sin^2\zeta}, \tag{4.7}$$

where ε is the prism angle and n_p is the refractive index of the prism. Figure 4.4 shows a prism coupling measurement result for an ALD-TiO_2 film, which is studied in Publication II. Using the matrix method as described in Section 3.2.1 and numerical optimization to find effective indices that match the three modes, a refractive index of 2.386 at 633 nm wavelength and a thickness of 452 nm can be found.

Loss measurements can also be done with a prism coupler by measuring the intensity of scattering from the waveguide as a function of distance with a multimode optical fiber. If we assume the waveguide to be uniform over the measured area, the losses can be determined by fitting an exponential function

$$f(D) = Ae^{-\alpha D/4.34}, \tag{4.8}$$

where D is the distance from a chosen zero-point, A the intensity at the zero-point, and α is the loss in dB/cm to the measured loss curve. Figure 4.5 shows the scattering intensity as a function of distance for an amorphous ALD-TiO_2 layer at 1.53 μm wavelength and a fitting curve with

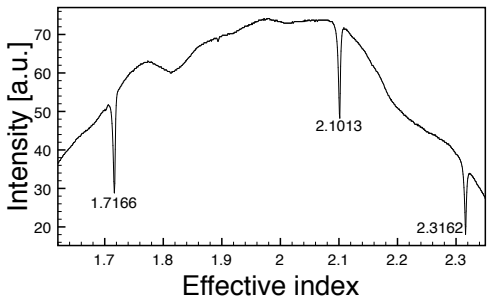

Figure 4.4. Prism coupling measurements from a TiO_2 film on a glass substrate at a wavelength of 633 nm. The effective indices of the modes are shown next to the corresponding dips.

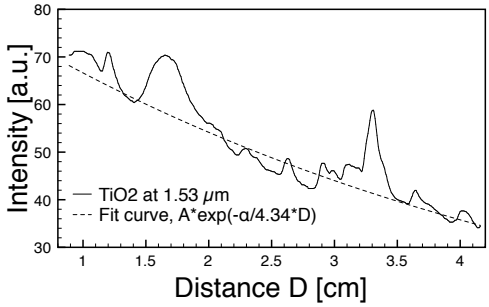

Figure 4.5. Scattering intensity as a function of distance D, with a fitted exponential function having $\alpha = 0.9$ dB/cm and $A = 82$.

$\alpha = 0.9$ dB/cm and $A = 82$.

4.4.4 Waveguide characterization

Light can be coupled from fibers to waveguides with various different schemes. Prism coupling, as explained in the previous section, can be used to couple light to slab waveguides but also to strip waveguides if a wide strip is used. The two most common coupling schemes for strip and slot waveguides are butt-coupling and grating-coupling.

In butt-coupling, the waveguides are cleaved and the end facet polished (depending on the material). In the case of nanowaveguides, the fibers are usually tapered and have a sharp tip to enable smaller mode area and better coupling efficiency. The waveguides can also be tapered or inverse tapered. The fibers are aligned with micropositioners to optimize the transmittance through the waveguides and minimize the coupling losses.

Grating couplers are waveguide gratings that are designed to couple light from a free-space beam or an optical fiber in a grazing incidence

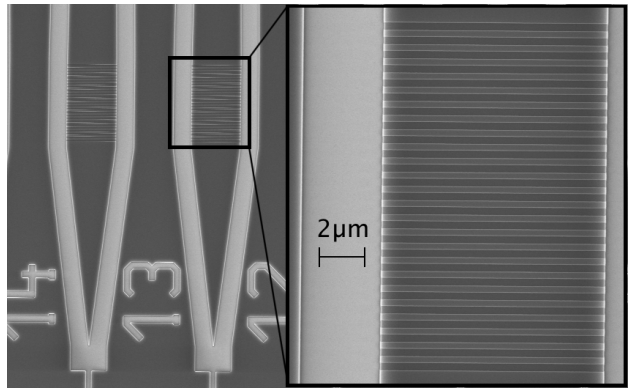

Figure 4.6. SEM image of a grating coupler etched onto an SOI wafer. The light gray areas are of SiO_2 and the dark gray areas are of Si. The gratings are etched only 70 nm from the surface, whereas the thickness of the Si layer is 220 nm.

angle to a waveguide mode or out from a waveguide mode [148]. Grating couplers do not require accurate cleaving or polishing of the chip and the chip can be designed to have multiple waveguide areas and the inputs and outputs do not have to be on the same line. Figure 4.6 shows an SEM image of the grating coupler design used on the chips in Publication III.

The intensity as a function of wavelength is usually the measured parameter and it is measured with different kinds of input sources and setups. The parameters that are usually of interest include the propagation losses and the transmittance as a function of wavelength.

4.4.5 Four-wave mixing

Four-wave mixing (FWM) is a well known nonlinear optical effect arising from the third-order $\chi^{(3)}$ coefficient [149, 150]. It is a mixing process that occurs if at least two waves interact in a nonlinear medium. Assuming just two input frequency components ω_1 and ω_2 (with $\omega_2 > \omega_1$), a refractive index modulation at the difference frequency occurs, which creates two additional frequency components: $\omega_3 = \omega_1 - (\omega_2 - \omega_1)$ and $\omega_4 = \omega_2 + (\omega_2 - \omega_1)$.

FWM is used to study the third-order ($\chi^{(3)}$) nonlinear properties of waveguides, and also as a spectroscopic tool. It can also be utilized in optical signal processing and it has to be taken into account when designing optical communication systems as it disturbs the signals.

5. Results

5.1 Optical properties of ALD-TiO_2

The properties of ALD grown materials depend on the deposition temperature and sometimes also slightly on the used pressure, flows, pulse and purge lengths. TiO_2 from $TiCl_4$ and H_2O is amorphous when it is grown below about 165 °C, anatase dominated at 165–350 °C, and rutile dominated at over 350 °C [18].

Polycrystalline films have usually rough surfaces and have grain boundaries that cause scattering losses. Birefringence can also cause scattering in waveguides, if the crystallites are not completely random. If we use a higher temperature of e.g. 350 °C for the TiO_2 process, the film will become crystalline as seen in Fig. 5.1a. However, the crystallinity can be controlled with intermediate amorphous films of e.g. Al_2O_3, which will limit the crystal size and the film will resemble the amorphous one as seen by comparing Fig. 5.1b and c. The films with intermediate Al_2O_3 layers made by trimethylaluminium/water process were absorbing and a different intermediate film chemistry has to be used if low loss films are wanted.

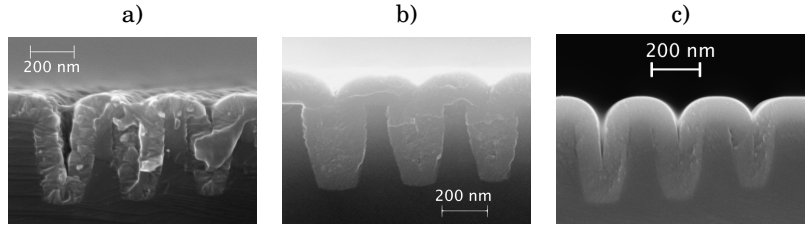

Figure 5.1. SEM pictures of TiO_2 films ALD deposited at 350 °C a) as is and b) with thin ($\sim$ 1 nm) intermediate Al_2O_3 layers, and at c) 120 °C into slot structures fabricated on silicon wafers.

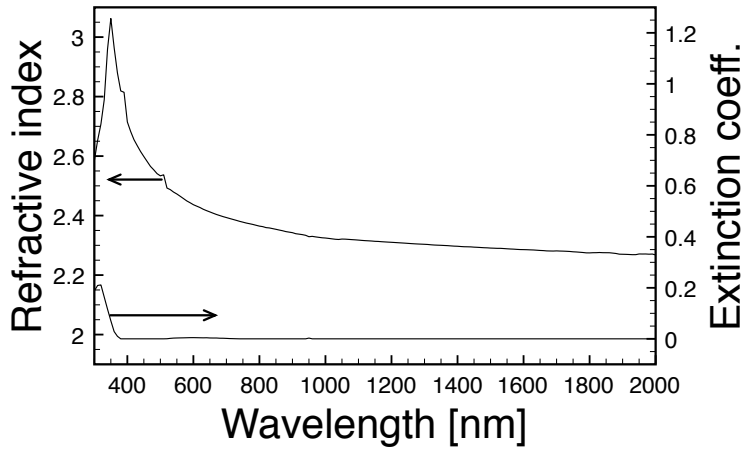

Figure 5.2. The refractive index and the extinction coefficient of ALD-TiO_2 deposited at 120 °C temperature as determined by spectroscopic ellipsometry.

Optical parameters of the ALD-TiO_2 films were determined using spectroscopic ellipsometry (SE) and prism coupling measurements. The TiO_2 sample used for SE measurement was from a different deposition run and the film thickness was much smaller. The films were deposited at 120 °C temperature.

A J. A. Woollam spectroscopic ellipsometer was used to measure the refractive index of the TiO_2 layer as a function of wavelength at a wavelength range of 300–2000 nm. Figure 5.2 shows the results.

A Metricon 2010 prism coupler was used to determine the propagation modes inside the films and to roughly estimate propagation losses of the films. The measurements were done at 633 nm and 1.53 μm wavelengths. The used prism coupler measures the dips in the intensity, corresponding the propagating modes, as a function of the incidence angle. The measured angles are then converted to corresponding effective indices. The refractive index and the thickness of the film can be determined using a 1-dimensional mode solver (e.g. the matrix method in Section 3.2.1).

Figure 5.3 shows the results from prism coupling measurements of TiO_2 films. The sharp peaks at both wavelengths indicate good optical properties. Using the matrix method as described in Section 3.2.1 and numerical optimization to find effective indices that match the three modes, a refractive index of 2.386 at 633 nm wavelength and a thickness of 452 nm is found. The refractive index for the 1.53 μm wavelength is 2.27, when the same thickness of 452 nm is used.

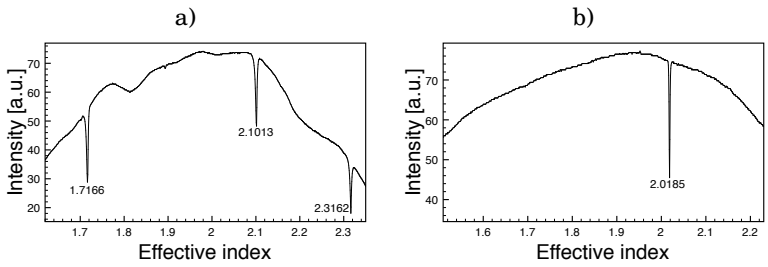

Figure 5.3. Prism coupling measurements from a TiO_2 film a) at 633 nm and b) at 1.53 μm wavelength on a glass substrate. The effective indices of the modes are shown next to the corresponding dips.

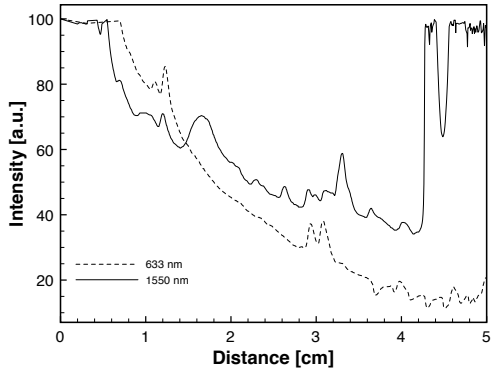

Figure 5.4. Intensity as a function of distance as measured by the Metricon fiber loss measurement add-on from the TiO_2 films at 633 nm and 1.53 μm wavelengths.

The propagation losses for TiO_2 were measured using the loss measurement option of the prism coupler. The results are shown in Fig. 5.4. For the TiO_2 film the Metricon bundled software gave values between 2–3.5 dB/cm at 633 nm and 0.8–0.9 dB/cm at 1.53 μm wavelength.

The prism coupling and SE measurements show a good agreement, although some variation could be expected due to slightly different substrate and deposition conditions.

The properties of low temperature TiO_2 are strongly dependent on the deposition temperature and the pulsing times, and are not completely saturating [19]. Figure 5.5 shows the refractive index and growth rate of TiO_2 as a function of temperature. The growth rate is higher at lower temperatures, and the chlorine content increases as well [19].

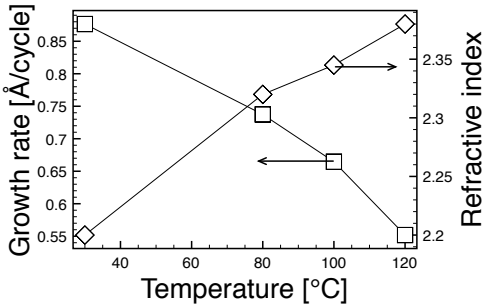

Figure 5.5. Growth rate and refractive index of TiO_2 as a function of temperature as measured by a Plasmos single wavelength ellipsometer at 633 nm wavelength.

5.2 Narrowing silicon slot waveguides with ALD-TiO_2

We proposed ALD as a method to narrow slot waveguide geometries in Publication I. If we start with 180 nm wide rails, 200 nm wide slot, and 220 nm thick Si device layer, we do not have any propagating modes in the Si waveguide. Figure 5.6 shows a schematic of a slot waveguide, for which the effective indices as a function of the TiO_2 layer thickness d are calculated in Fig. 5.7. The effective indices of the modes below $d = 30$ nm are below the refractive index of buried oxide, which means that the modes are leaky. Figure 5.8 shows the propagation losses for waveguides with similar dimensions as measured in Publication III. Two slot waveguides with similar starting geometries coated with 30 nm and 50 nm thick layers of TiO_2 are shown in Fig. 5.9.

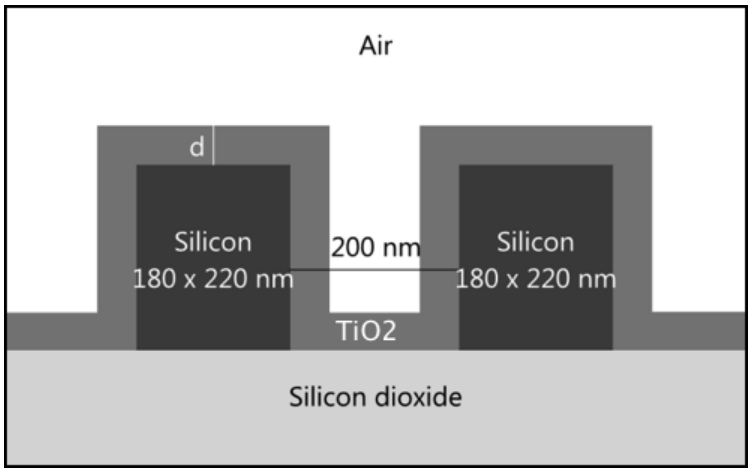

Figure 5.6. Schematic of a cross-section of a silicon slot waveguide coated with an ALD-TiO_2 layer of thickness d.

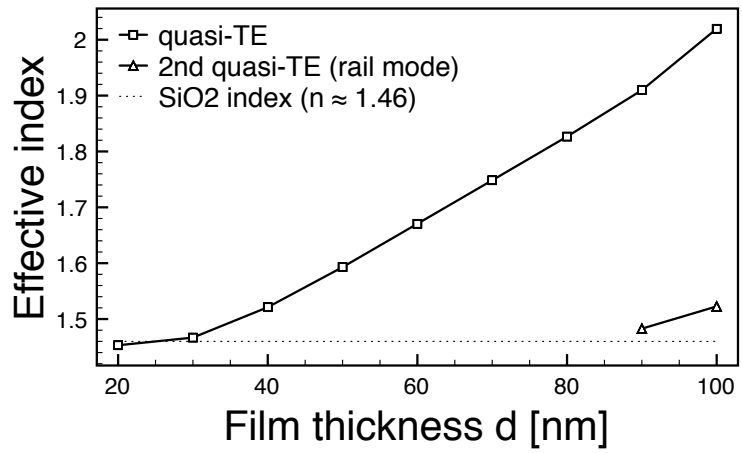

Figure 5.7. Effective index of the slot waveguide as a function of the TiO_2 layer thickness d.

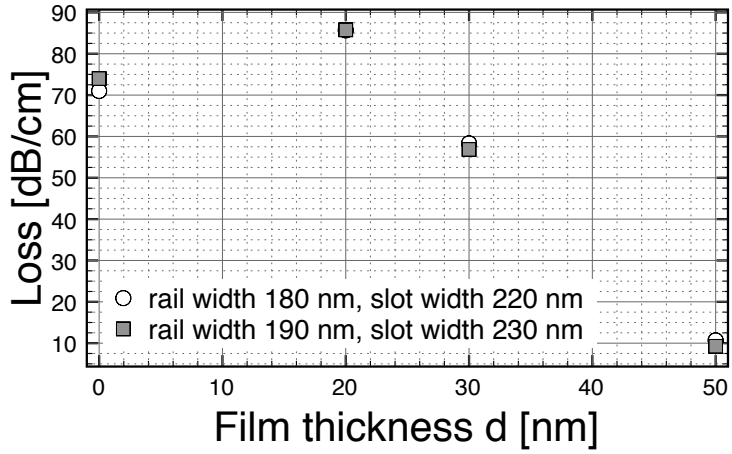

Figure 5.8. Propagation loss as a function of TiO_2 layer thickness d.

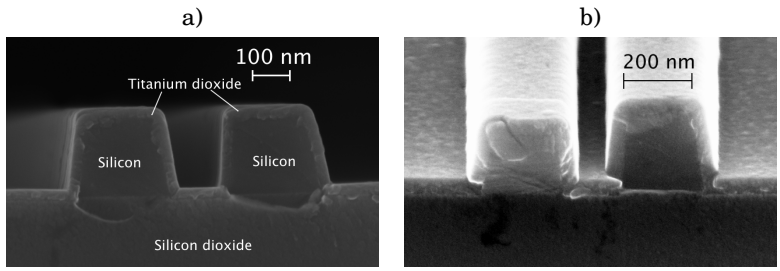

Figure 5.9. Scanning electron microscope (SEM) cross-section images of a silicon slot waveguides with similar starting geometries ALD-coated with a) 30 nm, and b) 50 nm thick layers of TiO_2. The left rail in image (b) has a slanted cleaving profile, which distorts the actual geometry.

5.3 Loss reduction by ALD-TiO_2 in silicon waveguides

In the previous section I showed that a weakly guiding or nonguiding silicon slot waveguide can be turned to a well-guiding one by adding a conformal layer of ALD-TiO_2. In Publication III we show experimentally that a larger TiO_2 cover thickness reduces the loss also when two well-guiding slot waveguides are compared.

In Section 3.2.5, we showed that the loss coefficient is proportional to the square of the modal field at the core-cladding boundary $\varphi^2(d)$ and also to the surface roughness σ^2 (the constant factor can be taken out of the Fourier transform of the autocorrelation function and its integral in Eq. 3.35). Figure 5.10 shows the measured propagation losses as a function of the air slot width and Fig. 5.11 shows the lateral electric field E_x for the same slot waveguide parameters. The mode field $\varphi(d)$ is proportional to E_x which is proportional to the air slot width. E_x is slightly stronger for the case with $d = 30$ nm if the rail widths w_r and slot widths w_s after the coating are kept the same. However, the losses are lower also for the $d = 50$ nm and the air slot width $w_s \approx 85$ nm cases, which have stronger $\varphi(d)$ than the cases with $d = 30$ nm and $w_s \approx 105$ nm, which would suggest that also the surface roughness is reduced.

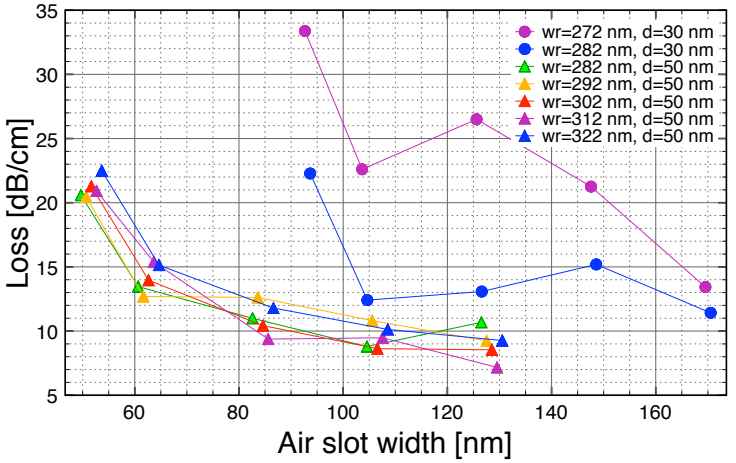

Figure 5.10. Measured propagation loss of well-guiding ($n_{\text{eff}} > 1.55$) slot waveguides as a function of the air slot width remaining after ALD-coating. The legend specifies the rail widths w_r after coating and the coating thicknesses d. The slot waveguide with thicker coating has lower losses, especially with the narrow air gaps.

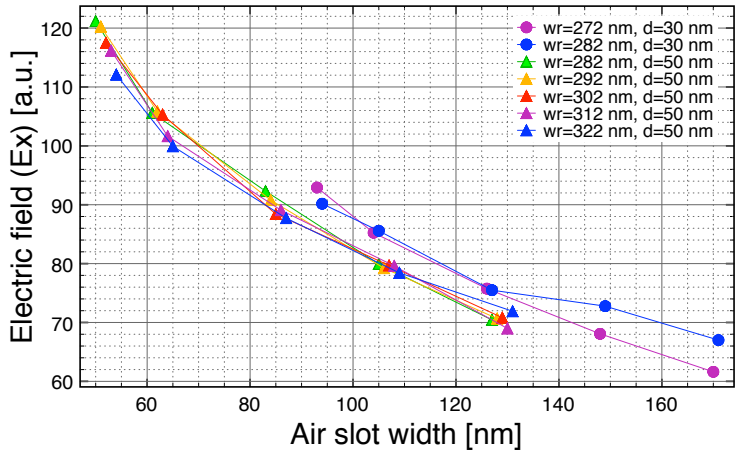

Figure 5.11. Calculated E_x at the TiO_2-air interface in the middle of the slot waveguide for the same slot waveguide parameters as in Fig. 5.10. The legend specifies the rail widths w_r after coating and the coating thicknesses d.

5.4 Angled sidewalls and filling of slot waveguides with ALD-TiO_2

The effect of angled sidewalls on the properties of silicon slot waveguides was discussed in Publication II. An enhanced vertical confinement was obtained with certain waveguide parameters. The reduced effective mode area was shown to enhance nonlinear effects in the waveguide and the use of ALD in realization of filled slot waveguides optimized for all-optical functionalities was discussed.

Figure 5.12 shows a completely filled slot waveguide. We were able to

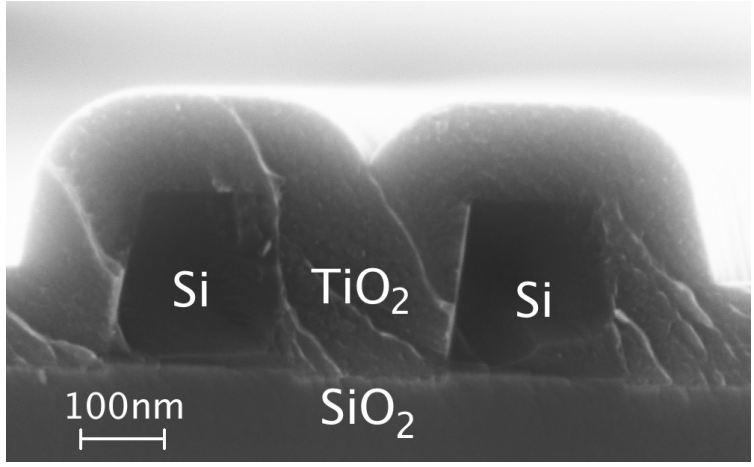

Figure 5.12. SEM image of a cross section of a completely TiO_2 filled slot waveguide. The same chips as in Publication III were used.

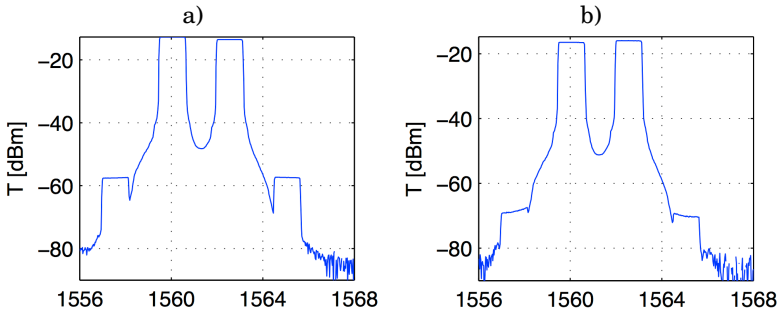

Figure 5.13. Four-wave mixing (FWM) measurements from a) a 500 nm wide silicon strip waveguide and b) a silicon slot waveguide with 230 nm wide rails and a 160 nm wide slot, both ALD-coated with a 120 nm thick layer of TiO_2. The two peaks at ∼1560 nm and ∼1563 nm are the input wavelengths and the side-peaks at ∼1557 nm and ∼1565 nm are generated by the FWM effect. The side-peaks are stronger for higher nonlinearities.

generate and measure four-wave mixing (FWM) in the filled TiO_2 waveguides, but as expected the best TiO_2 filled silicon slot waveguides showed less nonlinearity than the best strip waveguides as shown in Fig. 5.13. This is because $\chi^{(3)}$ of TiO_2 is smaller than that of silicon, though high for an oxide (about 50 times higher than of silica [151]).

Nevertheless, because of the relatively high $\chi^{(3)}$ and the vanishing nonlinear loss (α_2) of TiO_2, the slot waveguide is expected to improve the $\chi^{(3)}/\alpha_2$ figure of merit (FOM) for nonlinear applications [152, 153, Publication II], although it is still smaller than for the best nonlinear organic materials. Unfortunately, the limitations in the grating coupler design did not allow us to carry out loss measurements for the completely TiO_2 filled slot waveguides, and we were not able to experimentally measure the $\chi^{(3)}/\alpha_2$ figure of merit for these waveguides. A higher FOM might be realized by combining the narrowing and loss reduction effects of an ALD-TiO_2 layer with a highly nonlinear organic filling material.

5.5 Absorbing and wide-band resonant waveguide gratings

In Publication IV, it was shown that ALD-TiO_2 is a suitable material for fabricating high-quality resonant waveguide gratings. We introduced resonant absorbing metal-dielectric gratings, where metallic wires are embedded inside a titanium oxide grating in Publication V. The structure, as shown in Fig. 5.14, was made by two separate ALD coating steps, with

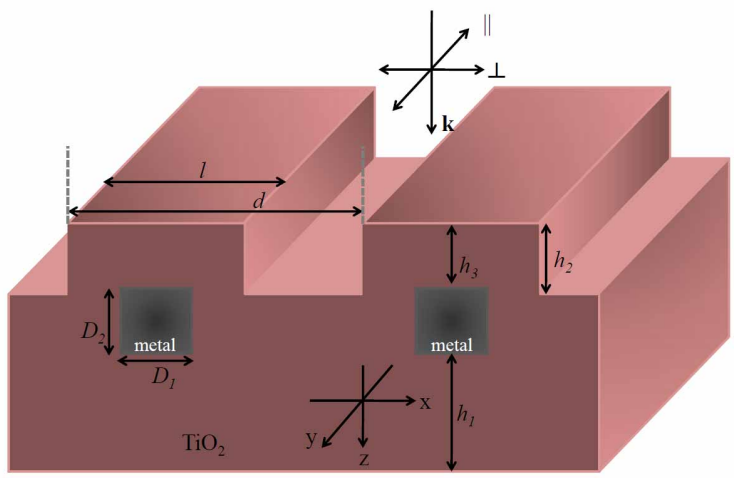

Figure 5.14. Schematic of the grating geometry. The structure is fabricated by first ALD-depositing the bottom TiO_2 layer, then depositing and patterning the metal, and finally depositin the second ALD-TiO_2 layer. [From Publication V]

the metal deposition and patterning step in between. The guided-mode resonance was shown to yield an almost total absorption of one polarization component in a thin structure, as the structure greatly enhances the absorption in localized surface plasma resonance. The structures have potential to function as filters or polarizing beamsplitters.

Semi-wideband resonant waveguide gratings for visible wavelengths were realized using the high refractive index and low absorption of the amorphous ALD-TiO_2 films in Publication VI. A very good agreement with the theoretical predictions and the experimental results was shown. The resonance grating provides approximately 20–30 nm bandwidth with over 90% reflectance at the visible wavelengths. These kind of reflectors may be useful in applications that make use of wider bandwidth light sources like LEDs.

5.6 Resonant waveguide gratings from an azobenzene polymer

We fabricated resonant waveguide gratings (RWG) by ALD-coating photoinduced surface-relief gratings on P4VP(OH-DMA)$_{0.33}$ azobenzene polymer complex [1, 8]. The grating fabrication process is explained in Section 4.2. An example of such a grating on a Si substrate is shown in Fig. 5.15.

The waveguiding TiO_2 layer was deposited at 80 °C on the surface-relief grating using ALD. At higher temperatures, the surface-relief grating

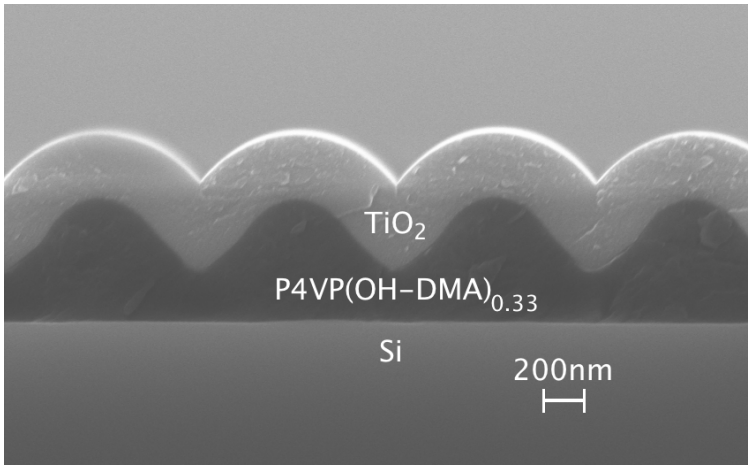

Figure 5.15. SEM image of a cross-section of a sinusoidal resonant-waveguide grating made by coating a photoinduced surface-relief grating with ALD-TiO_2.

would have been erased through thermal effects as shown in Fig. 5.16. The TiO_2 layer improved the thermal performance, and after the coating the diffraction efficiency was stable up to 200 °C compared to 90 °C before the ALD. Some cracks were formed onto the TiO_2-coated grating upon heating over 90 °C, but they didn't affect the diffraction efficiency. Instead, the efficiency improved probably because the refractive index of the TiO_2 layer rises upon heating.

Figure 5.17 shows the transmittance of an azobenzene RWG with a period of approximately 970 nm, a depth of 450 nm, and a 340 nm thick ALD-TiO_2 layer, on a glass substrate. The sharpest resonance peak is for the TE polarization at 1650 nm wavelength, where the transmittance reaches a value of only 0.4 %. No clear absorption is seen in the transmittance curve through the as-spinned polymer film above the absorbing edge at $\sim$550 nm wavelength, so the non-transmitted light is expected to be almost completely reflected from the grating.

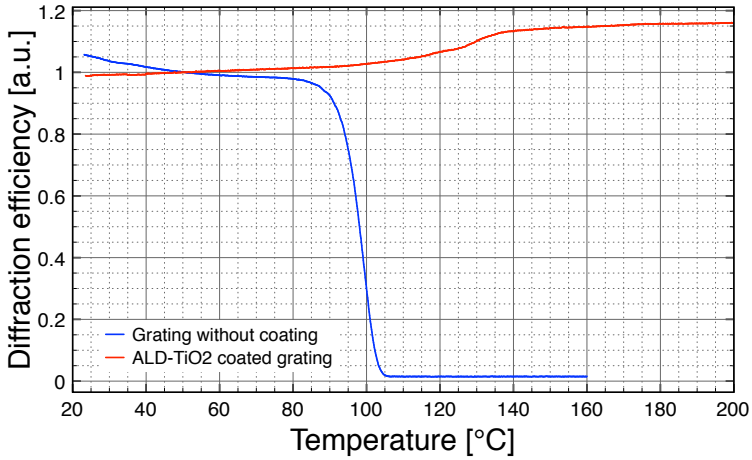

Figure 5.16. Normalized diffraction efficiency as a function of temperature for a photoinduced grating made on P4VP(OH-DMA)$_{0.33}$, with and without ALD-TiO_2 overlayer.

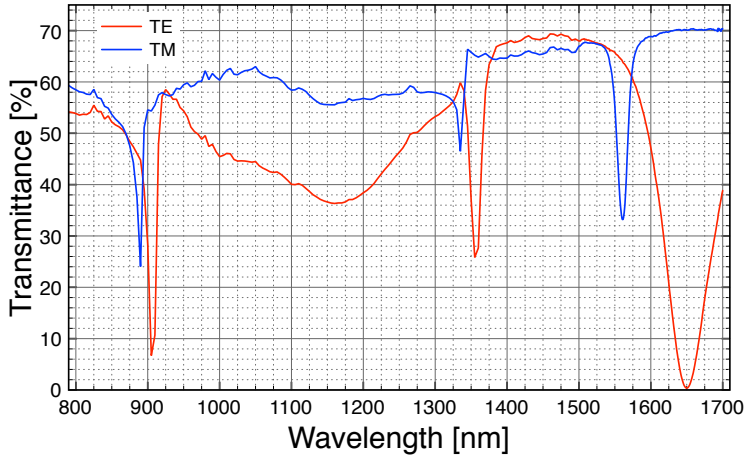

Figure 5.17. Transmittance for the TE and TM polarizations in a direct incidence through an azobenzene RWG with approximately 970 nm period, 450 nm depth, and a 340 nm thick ALD-TiO_2 layer on a glass substrate.

6. Summary and outlook

This study focused on the optical properties of atomic layer deposited (ALD) amorphous titanium dioxide (TiO_2) and its application in photonic devices, namely waveguides and diffraction gratings. The optical and waveguiding properties of amorphous TiO_2, deposited at a relatively low temperature of 120 °C, were studied and it was found to be a suitable material to narrow silicon slot waveguides and also to reduce the propagation losses. The optical quality of amorphous TiO_2 was proved to be good enough to fabricate high-quality resonant waveguide gratings.

The refractive index of amorphous ALD-TiO_2, which was deposited at 120 °C temperature, was 2.27 at a $\sim$1.55 μm wavelength and the losses of TiO_2 slab waveguides on glass at the same wavelength were below 1 dB/cm [Publication IV]. Using ALD-TiO_2 for narrowing down slot waveguides was introduced in Publication I. The idea proved to be useful as the silicon slot waveguides fabricated in Publication III did not work without a coating. Furthermore, a reduction of losses in silicon strip and slot waveguides by the ALD-TiO_2 coating was shown. The effects of angled sidewalls, a result of the etching, were studied and the complete filling of slot waveguides with TiO_2 was proposed in Publication II. A four-wave mixing signal was measured for completely TiO_2-filled slot waveguides and TiO_2-coated strip waveguides. An even higher nonlinear performance is expected if a silicon slot waveguide narrowed with ALD-TiO_2 is filled with a highly nonlinear organic material.

ALD-TiO_2 was also used to successfully fabricate novel absorbing polarization selective resonant gratings [Publication V], and semi-wide bandwidth resonant waveguide reflectors [Publication VI]. A novel way of fabricating a resonant waveguide grating by applying an ALD-TiO_2 layer on a holographically written surface relief grating on an azobenzene polymer complex was introduced and the initial results are promising.

Low temperature ALD-TiO_2 can be used as an alternative to more commonly used chemical vapor deposited (CVD) silicon nitride (Si_3N_4) in many optical applications and the growth mode of ALD can also enable smart fabrication strategies and completely new kind of structures. The TiO_2 ALD-grown in 120° has a higher refractive index of ∼2.4 than ∼2.0 of Si_3N_4 at visible wavelengths, and can thus provide higher refractive index contrast than the more commonly used Si_3N_4 in waveguides working at visible wavelengths.

This study has only touched the surface of what ALD-grown materials might provide in waveguiding applications. The studied amorphous ALD-TiO_2 material showed an excellent performance in all the studied applications, and will very probably see use in various photonic devices in the future. I am expecting many more interesting publications on application of ALD-TiO_2 in fabricating waveguides, gratings, and other photonic devices on various substrates in the future. Interesting results are also expected when ALD-films are used in tuning silicon waveguides and in combination with the silicon-organic-hybrid platform. The low growth temperature of ALD-TiO_2 allows the growth of waveguides on top of processed silicon microchips, and it might be a suitable material for building the optically interconnected microchips of the future.

Bibliography

[1] T. Alasaarela, D. Zheng, L. Huang, A. Priimagi, B. Bai, A. Tervonen, S. Honkanen, M. Kuittinen, and J. Turunen, Single-layer one-dimensional nonpolarizing guided-mode resonance filters under normal incidence. *Opt. Lett.*, In press.

[2] A. Säynätjoki, L. Karvonen, A. Khanna, T. Alasaarela, A. Tervonen, S. Honkanen, "Silicon slot waveguides for nonlinear optics", *Proc. SPIE*, vol. 7212, 72120T, 2009.

[3] T. Alasaarela, A. Säynätjoki, P. Stenberg, M. Kuittinen, S.Honkanen, "Filling of Slot Waveguides with Atomic Layer Deposition" (talk), *CLEO Europe -EQEC 2009*, Munich, Germany, June 14-19, Paper CK10.6, 2009.

[4] T. Alasaarela, A. Säynätjoki, P. Stenberg, M. Kuittinen, S. Honkanen, "Filling of Slot Waveguides with Versatile Material Systems Using Atomic Layer Deposition" (poster), *Integrated Photonics and Nanophotonics Research and Applications (IPNRA)*, Honolulu, Hawaii, USA, July 12-17, Paper JTuB4, 2009.

[5] A. Säynätjoki, T. Alasaarela, A. Khanna, L. Karvonen, A. Tervonen, S. Honkanen, "Advantages of Angled Sidewalls in Slot Waveguides" (talk), *Integrated Photonics and Nanophotonics Research and Applications (IPNRA)*, July 12-17, Honolulu, Hawaii, USA, Paper ITuE2, 2009.

[6] T. Alasaarela, J. Hiltunen, A. Khanna, A. Säynätjoki, A. Tervonen, S. Honkanen, "Optical properties of atomic layer deposited materials and their application in silicon waveguides", *Proc. SPIE*, vol. 7598, 75980D, 2010.

[7] A. Säynätjoki, T. Alasaarela, A. Khanna, A. Tervonen, S. Honkanen, "Mode properties of ALD filled silicon slot waveguides", Proc. SPIE vol. 7606, 76061G, 2010.

[8] T. Alasaarela, A. Priimägi, B. Bai, A. Tervonen, S. Honkanen, "Titanium dioxide coated photoinduced surface relief grating as a resonant waveguide grating" (talk), *CLEO Europe -EQEC 2011*, Munich, Germany, May 22-26, Paper CE8.1, 2011.

[9] B. Jalali and S. Fathpour, "Silicon photonics," *J. Lightwave Technol.*, vol. 24, no. 12, pp. 4600–4615, 2006.

[10] M. Lipson, "Guiding, modulating, and emitting light on silicon-challenges and opportunities," *J. Lightwave Technol.*, vol. 23, no. 12, pp. 4222–4238, 2005.

[11] A. Alduino and M. Paniccia, "Interconnects: Wiring electronics with light," *Nature Photon.*, vol. 1, no. 3, pp. 153–155, 2007.

[12] R. Puurunen, "Surface chemistry of atomic layer deposition: A case study for the trimethylaluminum/water process," *J. Appl. Phys.*, vol. 97, p. 121301, 2005.

[13] J. Aarik, A. Aidla, A. Kiisler, T. Uustare, and V. Sammelselg, "Effect of crystal structure on optical properties of TiO_2 films grown by atomic layer deposition," *Thin Sol. Films*, vol. 305, no. 1-2, pp. 270–273, 1997.

[14] M. Ritala, M. Leskelä, L. Niinistö, and T. Prohaska, "Surface roughness reduction in atomic layer epitaxy growth of titanium dioxide thin films," *Thin Sol. Films*, vol. 249, no. 22, pp. 155–162, 1994.

[15] J. Wang, X. Deng, R. Varghese, and A. Nikolov, "Filling high aspect-ratio nano-structures by atomic layer deposition and its applications in nano-optic devices and integrations," *J. Vac. Sci.*, vol. 23, no. 6, pp. 3209–3213, 2005.

[16] K. Kukli, H. Heikkinen, E. Nykänen, and L. Niinistö, "Deposition of lanthanum sulfide thin films by atomic layer epitaxy," *J. Alloys Comp.*, vol. 275-277, pp. 10–14, 1998.

[17] M. Ritala, M. Leskelä, E. Nykanen, P. Soininen, and L. Niinistö, "Growth of titanium dioxide thin films by atomic layer epitaxy," *Thin Sol. Films*, vol. 225, no. 1-2, pp. 288–295, 1993.

[18] J. Aarik, A. Aidla, T. Uustare, and V. Sammelselg, "Morphology and structure of TiO_2 thin films grown by atomic layer deposition," *J. Cryst. Growth*, vol. 148, no. 3, pp. 268–275, 1995.

[19] G. Triani, J. A. Campbell, P. J. Evans, J. Davis, B. A. Latella, and R. P. Burford, "Low temperature atomic layer deposition of titania thin films," *Thin Sol. Films*, vol. 518, no. 12, pp. 3182–3189, 2010.

[20] M. Ritala, M. Leskelä, L. Niinistö, and P. Haussalo, "Titanium isopropoxide as a precursor in atomic layer epitaxy of titanium dioxide thin films," *Chem. Mater.*, vol. 5, no. 8, pp. 1174–1181, 1993.

[21] M. Ritala, M. Leskelä, and E. Rauhala, "Atomic layer epitaxy growth of titanium dioxide thin films from titanium ethoxide," *Chem. Mater.*, vol. 6, no. 4, pp. 556–561, 1994.

[22] K. Kukli, M. Ritala, M. Schuisky, M. Leskelä, T. Sajavaara, J. Keinonen, T. Uustare, and A. Hårsta, "Atomic layer deposition of titanium oxide from TiI_4 and H_2O_2," *Chem. Vap. Deposition*, vol. 6, no. 6, pp. 303–310, 2000.

[23] T. Asikainen, M. Ritala, and M. Leskelä, "Growth of In_2S_3 thin films by atomic layer epitaxy," *Appl. Surf. Sci.*, vol. 82–83, pp. 122–125, 1994.

[24] N. Naghavi, R. Henriquez, V. Laptev, and D. Lincot, "Growth studies and characterisation of In_2S_3 thin films deposited by atomic layer deposition (ALD)," *Appl. Surf. Sci.*, vol. 222, pp. 65–73, 2004.

[25] A. Tarre, J. Aarik, H. Mandar, A. Niilisk, R. Parna, R. Rammula, T. Uustare, A. Rosental, and V. Sammelselg, "Atomic layer deposition of Cr_2O_3 thin films: Effect of crystallization on growth and properties," *Appl. Surf. Sci.*, vol. 254, no. 16, pp. 5149–5156, 2008.

[26] J. Ihanus, M. Ritala, M. Leskelä, and E. Rauhala, "ALE growth of $ZnS_{1-x}Se_x$ thin films by substituting surface sulfur with elemental selenium," *Appl. Surf. Sci.*, vol. 112, pp. 154–158, 1997.

[27] J. Ihanus, E. Lambers, P. H. Holloway, M. Ritala, and M. Leskelä, "XPS and electroluminescence studies on $SrS_{1-x}se_x$ and $ZnS_{1-x}se_x$ thin films deposited by atomic layer deposition technique," *J. Cryst. Growth*, vol. 260, no. 3-4, pp. 440–446, 2004.

[28] H. L. Lu, G. Scarel, M. Alia, M. Fanciulli, S.-J. Ding, and D. W. Zhang, "Spectroscopic ellipsometry study of thin NiO films grown on Si (100) by atomic layer deposition," *Appl. Phys. Lett.*, vol. 92, no. 22, p. 222907, 2008.

[29] K. Kukli, M. Ritala, M. Leskelä, and R. Lappalainen, "Niobium oxide thin films grown by atomic layer epitaxy," *Chem. Vap. Deposition*, vol. 4, no. 1, pp. 29–34, 1998.

[30] J. Ihanus, M. Ritala, M. Leskelä, T. Prohaska, R. Resch, G. Friedbacher, and M. Grasserbauer, "AFM studies on ZnS thin films grown by atomic layer epitaxy," *Appl. Surf. Sci.*, vol. 120, no. 1-2, pp. 43–50, 1997.

[31] D. Riihelä, M. Ritala, R. Matero, and M. Leskelä, "Introducing atomic layer epitaxy for the deposition of optical thin films," *Thin Sol. Films*, vol. 289, no. 1-2, pp. 250–255, 1996.

[32] M. Ylilammi and T. Ranta-aho, "Metal fluoride thin films prepared by atomic layer deposition," *J. Electrochem. Soc.*, vol. 141, no. 5, p. 1278, 1994.

[33] M. Ritala and M. Leskelä, "Zirconium dioxide thin films deposited by ALE using zirconium tetrachloride as precursor," *Appl. Surf. Sci.*, vol. 75, no. 1-4, pp. 333–340, 1994.

[34] K. Kukli, M. Ritala, and M. Leskelä, "Low-temperature deposition of zirconium oxide-based nanocrystalline films by alternate supply of $Zr[OC(CH_3)_3]_4$ and H_2O," *Chem. Vap. Deposition*, vol. 6, no. 6, pp. 297–301, 2000.

[35] K. Kukli, K. Forsgren, M. Ritala, M. Leskelä, J. Aarik, and A. Hårsta, "Dielectric properties of zirconium oxide grown by atomic layer deposition from iodide precursor," *J. Electrochem.Soc.*, vol. 148, no. 12, p. F227, 2001.

[36] K. Kukli, K. Forsgren, J. Aarik, T. Uustare, A. Aidla, A. Niskanen, M. Ritala, M. Leskelä, and A. Hårsta, "Atomic layer deposition of zirconium oxide from zirconium tetraiodide, water and hydrogen peroxide," *J. Cryst. Growth*, vol. 231, no. 1-2, pp. 262–272, 2001.

[37] R. Matero, M. Ritala, M. Leskelä, A. C. Jones, P. A. Williams, J. F. Bickley, A. Steiner, T. J. Leedham, and H. O. Davies, "Atomic layer deposition of ZrO_2 thin films using a new alkoxide precursor," *J. Non-cryst. Sol.*, vol. 303, no. 1, pp. 24–28, 2002.

[38] K. Kukli, J. Aarik, A. Aidla, O. Kohana, T. Uustare, and V. Sammelselg, "Properties of tantalum oxide thin films grown by atomic layer deposition," *Thin Sol. Films*, vol. 260, no. 2, pp. 135–142, 1995.

[39] J. Rautanen, M. Leskelä, L. Niinistö, E. Nykanen, P. Soininen, and M. Utriainen, "The effect of growth parameters on the deposition of CaS thin films by atomic layer epitaxy," *Appl. Surf. Sci.*, vol. 82-83, pp. 553–558, 1994.

[40] V. Saanila, J. Ihanus, M. Ritala, and M. Leskelä, "Atomic layer epitaxy growth of BaS and BaS:ce thin films from in situ synthesized $Ba(thd)_2$," *Chem. Vap. Deposition*, vol. 4, no. 6, pp. 227–233, 1998.

[41] J. Ihanus, T. Hänninen, T. Hatanpää, T. Aaltonen, I. Mutikainen, T. Sajavaara, J. Keinonen, M. Ritala, and M. Leskelä, "Atomic layer deposition of SrS and BaS thin films using cyclopentadienyl precursors," *Chem. Mater.*, vol. 14, no. 5, pp. 1937–1944, 2002.

[42] T. Asikainen, M. Ritala, and M. Leskelä, "Growth of In_2O_3 thin films by atomic layer epitaxy," *J. Electrochem.Soc.*, vol. 141, no. 11, pp. 3210–3213, 1994.

[43] M. Ritala, T. Asikainen, and M. Leskelä, "Enhanced growth rate in atomic layer epitaxy of indium oxide and indium-tin oxide thin films," *Electrochem. Solid-State Lett.*, vol. 1, no. 3, pp. 156–157, 1998.

[44] P. Soininen, E. Nykänen, L. Niinistö, and M. Leskelä, "Atomic layer epitaxy of strontium sulfide thin films using in situ synthesized strontium precursors," *Chem. Vap. Deposition*, vol. 2, no. 2, pp. 69–74, 1996.

[45] J. Klaus, A. W. Ott, A. C. Dillon, and S. M. George, "Atomic layer controlled growth of Si_3N_4 films using sequential surface reactions," *Surf. Sci.*, vol. 418, no. 1, pp. L14–L19, 1998.

[46] M. Vehkamäki, M. Ritala, M. Leskelä, A. C. Jones, H. O. Davies, T. Sajavaara, and E. Rauhala, "Atomic layer deposition of strontium tantalate thin films from bimetallic precursors and water," *J. Electrochem.Soc.*, vol. 151, no. 4, p. F69, 2004.

[47] M. Ritala, M. Leskelä, L. Niinistö, T. Prohaska, G. Friedbacher, and M. Grasserbauer, "Development of crystallinity and morphology in hafnium dioxide thin films grown by atomic layer epitaxy," *Thin Sol. Films*, vol. 250, no. 1-2, pp. 72–80, 1994.

[48] K. Kukli, M. Ritala, T. Sajavaara, J. Keinonen, and M. Leskelä, "Comparison of hafnium oxide films grown by atomic layer deposition from iodide and chloride precursors," *Thin Sol. Films*, vol. 416, no. 1-2, pp. 72–79, 2002.

[49] K. Kukli, M. Ritala, M. Leskelä, T. Sajavaara, J. Keinonen, A. C. Jones, and J. L. Roberts, "Atomic layer deposition of hafnium dioxide films from 1-methoxy-2-methyl-2-propanolate complex of hafnium," *Chem. Mater.*, vol. 15, no. 8, pp. 1722–1728, 2003.

[50] X. Liu, S. Ramanathan, A. Longdergan, A. Srivastava, E. Lee, T. E. Seidel, J. T. Barton, D. Pang, and R. G. Gordon, "ALD of hafnium oxide thin films from tetrakis(ethylmethylamino)hafnium and ozone," *J. Electrochem.Soc.*, vol. 152, no. 3, pp. G213–G219, 2005.

[51] J. Elam, Z. A. Sechrist, and S. M. George, "ZnO/Al_2O_3 nanolaminates fabricated by atomic layer deposition: growth and surface roughness measurements," *Thin Sol. Films*, vol. 414, no. 1, pp. 43–55, 2002.

[52] K. Elers, M. Ritala, M. Leskelä, and L. Johansson, "Atomic layer epitaxy growth of AlN thin films," *J. De Physique IV*, vol. 5, no. 5, pp. C5.1021–C5.1027, 1995.

[53] M. Putkonen, M. Nieminen, J. Niinistö, L. Niinistö, and T. Sajavaara, "Surface-controlled deposition of Sc_2O_3 thin films by atomic layer epitaxy using [beta]-diketonate and organometallic precursors," *Chem. Mater.*, vol. 13, no. 12, pp. 4701–4707, 2001.

[54] K. Kukli, T. Hatanpää, M. Ritala, and M. Leskelä, "Atomic layer deposition of gadolinium oxide films," *Chem. Vap. Deposition*, vol. 13, no. 10, pp. 546–552, 2007.

[55] M. Nieminen, S. Lehto, and L. Niinistö, "Atomic layer epitaxy growth of $LaGaO_3$ thin films," *J. Mat. Chem.*, vol. 11, no. 12, pp. 3148–3153, 2001.

[56] H. Viirola and L. Niinistö, "Controlled growth of tin dioxide thin films by atomic layer epitaxy," *Thin Sol. Films*, vol. 249, no. 2, pp. 144–149, 1994.

[57] J. Elam, D. Baker, A. Hryn, and A. Martinson, "Atomic layer deposition of tin oxide films using tetrakis (dimethylamino) tin," *J. Vac. Sci. Technol. A*, vol. 26, no. 12, pp. 244–252, 2008.

[58] H. Mölsä, L. Niinistö, and M. Utriainen, "Growth of yttrium oxide thin films from β-diketonate precursor," *Adv. Mater. Opt. Electron.*, vol. 4, no. 6, pp. 389–400, 1994.

[59] M. Putkonen, T. Sajavaara, L. Johansson, and L. Niinistö, "Low-temperature ALE deposition of Y_2O_3 thin films from β-diketonate precursors," *Chem. Vap. Deposition*, vol. 7, no. 1, pp. 44–50, 2001.

[60] M. Nieminen, L. Niinistö, and E. Rauhala, "Growth of gallium oxide thin films from gallium acetylacetonate by atomic layer epitaxy," *J. Mat. Chem.*, vol. 6, no. 1, pp. 27–31, 1996.

[61] T. Asikainen, M. Ritala, and M. Leskelä, "Growth of indium-tin-oxide thin films by atomic layer epitaxy," *J. Electrochem.Soc.*, vol. 142, no. 10, pp. 3538–3541, 1995.

[62] K. Kukli, M. Ritala, T. Pilvi, T. Sajavaara, M. Leskelä, A. C. Jones, H. C. Aspinall, D. C. Gilmer, and P. J. Tobin, "Evaluation of a praseodymium precursor for atomic layer deposition of oxide dielectric films," *Chem. Mater.*, vol. 16, no. 24, pp. 5162–5168, 2004.

[63] H. L. Lu, G. Scarel, L. Lamagna, M. Fanciulli, S.-J. Ding, and D. W. Zhang, "Effect of rapid thermal annealing on optical and interfacial properties of atomic-layer-deposited Lu_2O_3 films on Si (100)," *Appl. Phys. Lett.*, vol. 93, no. 15, p. 152906, 2008.

[64] M. Nieminen, T. Sajavaara, E. Rauhala, M. Putkonen, and L. Niinistö, "Surface-controlled growth of $LaAlO_3$ thin films by atomic layer epitaxy," *J. Mat. Chem.*, vol. 11, no. 9, pp. 2340–2345, 2001.

[65] K. Kukli, M. Ritala, V. Pore, M. Leskelä, T. Sajavaara, R. I. Hegde, D. C. Gilmer, P. Tobin, A. Jones, and H. Aspinall, "Atomic layer deposition and properties of lanthanum oxide and lanthanum-aluminum oxide films," *Chem. Vap. Deposition*, vol. 12, no. 2-3, pp. 158–164, 2006.

[66] K. Kukli, M. Ritala, T. Sajavaara, T. Hänninen, and M. Leskelä, "Atomic layer deposition of calcium oxide and calcium hafnium oxide films using calcium cyclopentadienyl precursor," *Thin Sol. Films*, vol. 500, no. 1-2, pp. 322–329, 2006.

[67] T. Hatanpää, J. Ihanus, J. Kansikas, I. Mutikainen, M. Ritala, and M. Leskelä, "Properties of $[Mg_2(thd)_4]$ as a precursor for atomic layer deposition of MgO thin films and crystal structures of $[Mg_2(thd)_4]$ and $[Mg(thd)_2(EtOH)_2]$," *Chem. Mater.*, vol. 11, no. 7, pp. 1846–1852, 1999.

[68] G. S. Higashi and C. G. Fleming, "Sequential surface chemical reaction limited growth of high quality Al_2O_3 dielectrics," *Appl. Phys. Lett.*, vol. 55, no. 19, p. 1963, 1989.

[69] K. Kukli, M. Ritala, and M. Leskelä, "Atomic layer epitaxy growth of aluminum oxide thin films from a novel $Al(CH_3)_2Cl$ precursor and H_2O," *J. Vac. Sci.*, vol. 15, no. 4, pp. 2214–2218, 1997.

[70] T. Pilvi, E. Puukilainen, K. Arstila, and M. Leskelä, "Atomic layer deposition of LaF_3 thin films using $La(thd)_3$ and TiF_4 as precursors," *Chem. Vap. Deposition*, vol. 14, no. 3-4, pp. 85–91, 2008.

[71] R. Matero, S. Haukka, and M. Tuominen, "High growth rate SiO_2 by atomic layer deposition," *ECS Trans.*, vol. 13, no. 1, pp. 453–457, 2008.

[72] T. Pilvi, K. Arstila, M. Leskelä, and M. Ritala, "Novel ALD process for depositing CaF_2 thin films," *Chem. Mater.*, vol. 19, no. 14, pp. 3387–3392, 2007.

[73] T. Pilvi, T. Hatanpää, E. Puukilainen, and K. Arstila, "Study of a novel ALD process for depositing MgF_2 thin films," *J. Mat. Chem.*, vol. 17, no. 48, pp. 5066–5083, 2007.

[74] T. Pilvi, E. Puukilainen, U. Kreissig, M. Leskelä, and M. Ritala, "Atomic layer deposition of MgF_2 thin films using TaF_5 as a novel fluorine source," *Chem. Mater.*, vol. 20, no. 15, pp. 5023–5028, 2008.

[75] A. Rugge, J. Becker, R. Gordon, and S. Tolbert, "Tungsten nitride inverse opals by atomic layer deposition," *Nano Lett.*, vol. 3, no. 9, pp. 1293–1297, 2003.

[76] J. King, C. Neff, C. Summers, W. Park, and S. Blomquist, "High-filling-fraction inverted ZnS opals fabricated by atomic layer deposition," *Appl. Phys. Lett.*, vol. 83, no. 13, pp. 2566–2568, 2003.

[77] M. Scharrer, X. Wu, A. Yamilov, H. Cao, and R. Chang, "Fabrication of inverted opal ZnO photonic crystals by atomic layer deposition," *Appl. Phys. Lett.*, vol. 86, p. 151113, 2005.

[78] E. Graugnard, J. King, S. Jain, C. Summers, Y. Zhang-Williams, and I. C. Khoo, "Electric-field tuning of the bragg peak in large-pore TiO_2 inverse shell opals," *Phys. Rev. B*, vol. 72, p. 233105, 2005.

[79] A. Rugge, J. Park, R. Gordon, and S. Tolbert, "Tantalum (v) nitride inverse opals as photonic structures for visible wavelengths," *J. Phys. Chem. B*, vol. 109, no. 9, pp. 3764–3771, 2005.

[80] J. King, E. Graugnard, and C. Summers, "TiO_2 inverse opals fabricated using low-temperature atomic layer deposition," *Adv. Mater.*, vol. 17, no. 8, pp. 1010–1013, 2005.

[81] M. Scharrer, X. Wu, A. Yamilov, H. Cao, and R. Chang, "Fabrication of inverted opal ZnO photonic crystals by atomic layer deposition," *Appl. Phys. Lett.*, vol. 86, p. 151113, 2005.

[82] J. King, D. Heineman, E. Graugnard, and C. Summers, "Atomic layer deposition in porous structures: 3d photonic crystals," *Appl. Surf. Sci.*, vol. 244, pp. 511–516, 2005.

[83] Z. Sechrist, B. Schwartz, J. Lee, and J. McCormick, "Modification of opal photonic crystals using Al_2O_3 atomic layer deposition," *Chem. Mater.*, vol. 18, no. 15, 2006.

[84] J. S. King, E. Graugnard, O. M. Roche, D. N. Sharp, J. Scrimgeour, R. Denning, A. Turberfield, and C. Summers, "Infiltration and inversion of holographically defined polymer photonic crystal templates by atomic layer deposition," *Adv. Mater.*, vol. 18, pp. 1561–1565, 2006.

[85] J. King, D. Gaillot, E. Graugnard, and C. Summers, "Conformally back-filled, non-close-packed inverse-opal photonic crystals," *Adv. Mater.*, vol. 18, pp. 1063–1067, 2006.

[86] M. Scharrer, A. Yamilov, X. Wu, H. Cao, and R. Chang, "Ultraviolet lasing in high-order bands of three-dimensional ZnO photonic crystals," *Appl. Phys. Lett.*, vol. 88, p. 201103, 2006.

[87] J. King, E. Graugnard, and C. Summers, "Photoluminescence modification by high-order photonic bands in TiO_2 / ZnS:Mn multilayer inverse opals," *Appl. Phys. Lett.*, vol. 88, p. 081109, 2006.

[88] D. Gaillot and C. Summers, "Photonic band gaps in non-close-packed inverse opals," *J. Appl. Phys.*, vol. 100, p. 113118, 2006.

[89] E. Graugnard, D. Gaillot, S. Dunham, and C. Neff, "Photonic band tuning in two-dimensional photonic crystal slab waveguides by atomic layer deposition," *Appl. Phys. Lett.*, vol. 89, p. 181108, 2006.

[90] E. Graugnard, V. Chawla, D. Lorang, and C. Summers, "High filling fraction gallium phosphide inverse opals by atomic layer deposition," *Appl. Phys. Lett.*, vol. 89, p. 211102, 2006.

[91] M. Scharrer, A. Yamilov, X. Wu, H. Cao, and R. Chang, "Ultraviolet lasing in high-order bands of three-dimensional ZnO photonic crystals," *Appl. Phys. Lett.*, vol. 88, p. 201103, 2006.

[92] E. Graugnard, J. King, D. Gaillot, and C. Summers, "Sacrificial-layer atomic layer deposition for fabrication of non-close-packed inverse-opal photonic crystals," *Adv. Funct. Mat.*, vol. 16, pp. 1187–1196, 2006.

[93] I. Povey, D. Whitehead, K. Thomas, and M. Pemble, "Photonic crystal thin films of gaas prepared by atomic layer deposition," *Appl. Phys. Lett.*, vol. 89, p. 104103, 2006.

[94] D. Gaillot, E. Graugnard, J. Blair, and C. Summers, "Dispersion control in two-dimensional superlattice photonic crystal slab waveguides by atomic layer deposition," *Appl. Phys. Lett.*, vol. 91, p. 181123, 2007.

[95] C. Yang, S. Wang, S. Liang, Y. Chang, and C. Chen, "Low-temperature growth of ZnO nanorods in anodic aluminum oxide on Si substrate by atomic layer deposition," *Appl. Phys. Lett.*, vol. 90, p. 033104, 2007.

[96] J. Lee, W. Leung, J. Ahn, T. Lee, I. Park, K. Constant, and K.-M. Ho, "Layer-by-layer photonic crystal fabricated by low-temperature atomic layer deposition," *Appl. Phys. Lett.*, vol. 90, p. 151101, 2007.

[97] I. Povey, M. Bardosova, F. Chalvet, and M. Pemble, "Atomic layer deposition for the fabrication of 3d photonic crystals structures: Growth of Al_2O_3 and VO_2 photonic crystal systems," *Surf. Coat. Technol.*, vol. 201, pp. 9345–9348, 2007.

[98] K. Solehmainen, M. Kapulainen, P. Heimala, and K. Polamo, "Erbium-doped waveguides fabricated with atomic layer deposition method," *IEEE Photon. Technol. Lett.*, vol. 16, no. 1, pp. 194–196, 2004.

[99] L. Norin, E. Vanin, P. Soininen, and M. Putkonen, "Atomic layer deposition as a new method for rare-earth doping of optical fibers," *Optical Society of America-CLEO/QELS Conference*, 2007.

[100] M. Born and E. Wolf, *Principles of Optics: Electromagnetic Theory of Propagation, Interference and Diffraction of Light*, 6th ed. Cambridge University Press, 1997.

[101] A. Yariv and Y. Pochi, *Photonics - Optical Electronics in Mordern Communications*. Oxford University Press, 2007.

[102] J. Chilwell and I. Hodkinson, "Thin-films field-transfer matrix theory of planar multilayer waveguides and reflection from prism-loaded waveguides," *J. Opt. Soc. Am. A*, vol. 1, no. 7, pp. 742–753, 1984.

[103] J. Leuthold, C. Koos, and W. Freude, "Nonlinear silicon photonics," *Nature Photon.*, vol. 4, no. 8, pp. 535–544, 2010.

[104] K. D. Vos, I. Bartolozzi, E. Schacht, P. Bienstman, and R. Baets, "Silicon-on-insulator microring resonator for sensitive and label-free biosensing," *Opt. Express*, vol. 15, no. 12, pp. 7610–7615, 2007.

[105] V. R. Almeida, Q. Xu, C. A. Barrios, and M. Lipson, "Guiding and confining light in void nanostructure," *Opt. Lett.*, vol. 29, no. 11, pp. 1209–1211, 2004.

[106] Q. Xu, V. R. Almeida, R. R. Panepucci, and M. Lipson, "Experimental demonstration of guiding and confining light in nanometer-size low-refractive-index material," *Opt. Lett.*, vol. 29, no. 14, pp. 1626–1628, 2004.

[107] C. A. Barrios, K. B. Gylfason, B. Sánchez, A. Griol, H. Sohlström, M. Holgado, and R. Casquel, "Slot-waveguide biochemical sensor," *Opt. Lett.*, vol. 32, no. 21, pp. 3080–3082, 2007.

[108] C. A. Barrios, M. J. Bañuls, V. González-Pedro, K. B. Gylfason, B. Sánchez, A. Griol, A. Maquieira, H. Sohlström, M. Holgado, and R. Casquel, "Label-free optical biosensing with slot-waveguides," *Opt. Lett.*, vol. 33, no. 7, pp. 708–710, 2008.

[109] T. Claes, J. G. Molera, K. D. Vos, E. Schacht, R. Baets, and P. Bienstman, "Label-free biosensing with a slot-waveguide-based ring resonator in silicon on insulator," *IEEE Photon. J.*, vol. 1, no. 3, pp. 197–204, 2009.

[110] M. Koshiba, *Optical Waveguide Theory by the Finite Element Method*, 1st ed. Tokyo/Dordrecht: KTK Scientific Publishers/Kluwer Academic Publishers, 1992.

[111] A. B. Fallahkhair, K. S. Li, and T. E. Murphy, "Vector finite difference modesolver for anisotropic dielectric waveguides," *J. Lightwave Technol.*, vol. 26, no. 11, pp. 1423–1431, 2008.

[112] A. S. Sudbo, "Film mode matching: a versatile numerical method for vector mode field calculations in dielectric waveguides," *Pure Appl. Opt.*, vol. 2, pp. 211–233, 1993.

[113] *FIMMWAVE by Photon Design, http://www.photond.com/*.

[114] C. G. Poulton, C. Koos, M. Fujii, A. Pfrang, T. Schimmel, J. Leuthold, and W. Freude, "Radiation modes and roughness loss in high index-contrast waveguides," *J. Sel. Top. Quantum Electron.*, vol. 12, no. 6, pp. 1306–1321, 2006.

[115] F. P. Payne and J. P. R. Lacey, "A theoretical analysis of scattering loss from planar optical waveguides," *Opt. Quant. Electron.*, vol. 26, no. 10, pp. 977–986, 1994.

[116] K. K. Lee, D. R. Lim, H.-C. Luan, A. Agarwal, J. Foresi, and L. C. Kimerling, "Effect of size and roughness on light transmission in a Si/SiO_2 waveguide: Experiments and model," *Appl. Phys. Lett.*, vol. 77, no. 11, p. 1617, 2000.

[117] K. K. Lee, D. R. Lim, L. C. Kimerling, J. Shin, and F. Cerrina, "Fabrication of ultralow-loss Si/SiO_2 waveguides by roughness reduction," *Opt. Lett.*, vol. 26, no. 23, pp. 1888–1890, 2001.

[118] K. P. Yap, A. Delâge, J. Lapointe, B. Lamontagne, J. H. Schmid, P. Waldron, B. A. Syrett, and S. Janz, "Correlation of scattering loss, sidewall roughness and waveguide width in silicon-on-insulator (SOI) ridge waveguides," *J. Lightwave Technol.*, vol. 27, no. 18, pp. 3999–4008, 2009.

[119] D. Maystre, "A new general integral theory for dielectric coated gratings," *J. Opt. Soc. Am.*, vol. 68, no. 4, pp. 490–495, 1978.

[120] J. Chandezon, M. Dupuis, and G. Cornet, "Multicoated gratings: a differential formalism applicable in the entire optical region," *J. Opt. Soc. Am.*, vol. 72, no. 7, pp. 839–846, 1982.

[121] L. Li, "Use of fourier series in the analysis of discontinuous periodic structures," *J. Opt. Soc. Am. A*, vol. 13, no. 9, pp. 1870–1876, 1996.

[122] L. Li, "New formulation of the fourier modal method for crossed surface-relief gratings," *J. Opt. Soc. Am. A*, vol. 134, no. 10, pp. 2758–2767, 1997.

[123] J. Turunen, "Diffraction theory of microrelief gratings," in *Micro-optics: Elements, Systems and Applications*, H. Herzig, Ed. Taylor & Francis, London, 1997.

[124] R. Magnusson and S. S. Wang, "New principle for optical filters," *Appl. Phys. Lett.*, vol. 61, no. 9, pp. 1022–1024, 1992.

[125] S. S. Wang and R. Magnusson, "Theory and applications of guided-mode resonance filters," *Appl. Opt.*, vol. 32, no. 14, pp. 2606–2613, 1993.

[126] T. Vallius, P. Vahimaa, and J. Turunen, "Pulse deformations at guided-mode resonance filters," *Opt. Express*, vol. 10, no. 16, pp. 840–843, 2002.

[127] M. Siltanen, S. Leivo, P. Voima, M. Kauranen, P. Karvinen, P. Vahimaa, and M. Kuittinen, "Strong enhancement of second-harmonic generation in all-dielectric resonant waveguide grating," *Appl. Phys. Lett.*, vol. 91, no. 11, p. 111109, 2007.

[128] P. Karvinen, T. Nuutinen, O. Hyvärinen, and P. Vahimaa, "Enhancement of laser-induced fluorescence at 473 nm excitation with subwavelength resonant waveguide gratings," *Opt. Express*, vol. 16, no. 21, pp. 16 364–16 370, 2008.

[129] Y. Fang, A. M. Ferrie, N. H. Fontaine, J. Mauro, and J. Balakrishnan, "Resonant waveguide grating biosensor for living cell sensing," *Biophysical Journal*, vol. 91, no. 5, pp. 1925–1940, 2006.

[130] S. Franssila, *Introduction to Microfabrication*, 2nd ed. Wiley, 2010.

[131] A. Priimagi, J. Vapaavuori, F. Rodriguez, C. F. J. Faul, M. T. Heino, O. Ikkala, M. Kauranen, and M. Kaivola, "Hydrogen-bonded polymer–azobenzene complexes: Enhanced photoinduced birefringence with high temporal stability through interplay of intermolecular interactions," *Chem. Mater.*, vol. 20, no. 20, pp. 6358–6363, 2008.

[132] A. Priimägi, "Polymer–azobenzene complexes: from supramolecular concepts to efficient photoresponsive polymers," Ph.D. dissertation, Helsinki University of Technology, 2009.

[133] T. Suntola and J. Hyvarinen, "Atomic layer epitaxy," *Ann. Rev. Mater. Sci.*, vol. 15, pp. 177–194, 1985.

[134] C. Goodman and M. Pessa, "Atomic layer epitaxy," *J. Appl. Phys.*, vol. 60, no. 3, pp. R65–R81, 1986.

[135] S. George, A. Ott, and J. Klaus, "Surface chemistry for atomic layer growth," *J. Phys. Chem.*, vol. 100, no. 31, pp. 13 121–13 131, 1996.

[136] L. Niinistö, M. Ritala, and M. Leskelä, "Synthesis of oxide thin films and overlayers by atomic layer epitaxy for advanced applications," *Mat. Sci. Eng. B*, vol. 41, pp. 23–29, 1996.

[137] M. Leskelä and M. Ritala, "ALD precursor chemistry: Evolution and future challenges," *J. De Physique IV*, vol. 9, no. 2, pp. Pr8.837–Pr8.852, 1999.

[138] M. Ritala and M. Leskelä, *Handbook of Thin Film Materials: Deposition and processing of thin films*. Academic Press, 2002, vol. 1, ch. 2.

[139] M. Ritala and J. Niinistö, *Chemical Vapor Deposition: Precursors, Processes and Applications*. Royal Society of Chemistry, 2009, ch. 4.

[140] M. Knez, K. Nielsch, and L. Niinistö, "Synthesis and surface engineering of complex nanostructures by atomic layer deposition*," *Adv. Mater.*, vol. 19, no. 21, pp. 3425–3438, 2007.

[141] H. Kim, H. Lee, and W. Maeng, "Applications of atomic layer deposition to nanofabrication and emerging nanodevices," *Thin Sol. Films*, vol. 517, no. 8, pp. 2563–2580, 2008.

[142] D. Hausmann, J. Becker, S. Wang, and R. Gordon, "Rapid vapor deposition of highly conformal silica nanolaminates," *Science*, vol. 298, no. 5592, pp. 402–406, 2002.

[143] J. Aarik, A. Aidla, H. Mandar, and T. Uustare, "Atomic layer deposition of titanium dioxide from $TiCl_4$ and H_2O: investigation of growth mechanism," *Appl. Surf. Sci.*, vol. 172, no. 1-2, pp. 148–158, 2001.

[144] J. J. Wang, A. Nikolov, and Q. Wu, "Nano- and microlens arrays grown using atomic-layer deposition," *IEEE Photon. Technol. Lett.*, vol. 18, no. 24, pp. 2650–2652, 2006.

[145] D. Marquardt, "An algorithm for least-squares estimation of nonlinear parameters," *SIAM J. Appl. Math.*, vol. 11, no. 2, pp. 431–441, 1963.

[146] P. K. Tien, "Light waves in thin films and integrated optics," *Appl. Opt.*, vol. 10, no. 11, pp. 2395–2413, 11.

[147] R. Ulrich and R. Torge, "Measurement of thin film parameters with a prism coupler," *Appl. Opt.*, vol. 12, no. 12, pp. 2901–2908, 1973.

[148] M. L. Dakss, L. Kuhn, P. F. Heidrich, and B. Scott, "Grating coupler for efficient excitation of optical guided waves in thin films," *Appl. Phys. Lett.*, vol. 16, no. 12, pp. 523–525, 1970.

[149] P. D. Maker and R. W. Terhune, "Study of optical effects due to an induced polarization third order in the electric field strength," *Phys. Rev.*, vol. 137, no. 3A, pp. A801–A818, 1965.

[150] J.-L. Oudar and Y. R. Shen, "Nonlinear spectroscopy by multiresonant four-wave mixing," *Phys. Rev. A*, vol. 22, no. 3, pp. 1141–1158, 1980.

[151] R. Adair, L. Chase, and S. Payne, "Nonlinear refractive index of optical crystals," *Phys. Rev. B*, vol. 39, no. 5, pp. 3337–3350, 1989.

[152] T. Vallaitis, S. Bogatscher, L. Alloatti, P. Dumon, R. Baets, M. L. Scimeca, I. Biaggio, F. Diederich, C. Koos, W. Freude, and J. Leuthold, "Optical properties of highly nonlinear silicon-organic hybrid (soh) waveguide geometries," *Opt. Express*, vol. 17, no. 20, pp. 17 357–17 368, 2009.

[153] C. Koos, P. Vorreau, T. Vallaitis, P. Dumon, W. Bogaerts, R. Baets, B. Esembeson, I. Biaggio, T. Michinobu, F. Diederich, W. Freude, and J. Leuthold, "All-optical high-speed signal processing with silicon-organic hybrid slot waveguides," *Nature Photon.*, vol. 3, no. 4, pp. 216–219, 2009.

Aalto-DD 57/2011

ISBN 978-952-60-4180-3 (pdf)
ISBN 978-952-60-4179-7
ISSN-L 1799-4934
ISSN 1799-4942 (pdf)
ISSN 1799-4934

Aalto University
School of Electrical Engineering
Department of Micro- and Nanosciences
www.aalto.fi

BUSINESS + ECONOMY

ART + DESIGN + ARCHITECTURE

SCIENCE + TECHNOLOGY

CROSSOVER

DOCTORAL DISSERTATIONS